DEVELOPMENT OF A MODULAR CONTROL ALGORITHM FOR HIGH PRECISION POSITIONING SYSTEMS

A THESIS

SUBMITTED TO THE DEPARTMENT OF MECHANICAL

ENGINEERING

AND THE GRADUATE SCHOOL OF ENGINEERING AND SCIENCE

OF BILKENT UNIVERSITY

IN PARTIAL FULFILLMENT OF THE REQUIREMENTS

FOR THE DEGREE OF

MASTER OF SCIENCE

By

Nurcan Geçer Ulu

August, 2012

I certify that I have read this thesis and that in my opinion it is fully adequate, in scope and in quality, as a thesis for the degree of Master of Science.

_____

Assist. Prof. Dr. Melih Çakmakcı (Advisor)

I certify that I have read this thesis and that in my opinion it is fully adequate, in scope and in quality, as a thesis for the degree of Master of Science.

_____

Assist. Prof. Dr. Yiğit Karpat

I certify that I have read this thesis and that in my opinion it is fully adequate, in scope and in quality, as a thesis for the degree of Master of Science.

_____

Prof. Dr. Hitay Özbay

Approved for the Graduate School of Engineering and Science:

_____

Prof. Dr. Levent Onural
Director of the Graduate School

ABSTRACT

DEVELOPMENT OF A MODULAR CONTROL ALGORITHM FOR HIGH PRECISION POSITIONING SYSTEMS

Nurcan Geçer Ulu
M.S. in Mechanical Engineering
Supervisor: Assist. Prof. Dr. Melih Çakmakcı
August, 2012

In the last decade, micro/nano-technology has been improved significantly. Micro/nano-technology related products started to be used in consumer market in addition to their applications in the science and technology world. These developments resulted in a growing interest for high precision positioning systems since precision positioning is crucial for micro/nano-technology related applications. With the rise of more complex and advanced applications requiring smaller parts and higher precision performance, demand for new control techniques that can meet these expectations is increased.

The goal of this work is developing a new control technique that can meet increased expectations of precision positioning systems. For this purpose, control of a modular multi-axis positioning system is studied in this thesis. The multi-axis precision positioning system is constructed by assembling modular single-axis stages. Therefore, a single-axis stage can be used in several configurations. Model parameters of a single-axis stage change depending on which axis it is used for. For this purpose, an iterative learning controller is designed to improve tracking performance of a modular single-axis stage to help modular sliders adapting to repeated disturbances and nonlinearities of the axis they are used for. When modular single-axis stages are assembled to form multi-axis systems, the interaction between the axes should be considered to operate stages simultaneously. In order to compensate for these interactions, a multi input multi output (MIMO) controller can be used such as cross-coupled controller (CCC). Cross-coupled controller examines the effects between axes by controlling the contour error resulting in an improved contour tracking.

In this thesis, a controller featuring cross-coupled control and iterative learning control schemes is presented to improve contour and tracking accuracy at the same time. Instead of using the standard contour estimation technique proposed with the variable gain cross-coupled control, presented control design incorporates a computationally efficient contour estimation technique. In addition to that, implemented contour estimation technique makes the presented control scheme more suitable for arbitrary nonlinear contours and multi-axis systems. Also, using the zero-phase filtering based iterative learning control results in a practical design and an increased applicability to modular systems. Stability and convergence of the proposed controller has been shown with the necessary theoretical analysis. Effectiveness of the control design is verified with simulations and experiments on two-axis and three-axis positioning systems. The resulting controller is shown to achieve nanometer level contouring and tracking performance.

ÖZET

YÜKSEK HASSASİYETLİ POZİSYONLAMA SİSTEMLERİ İÇİN MODÜLER KONTROL ALGORİTMASI GELİŞTİRİLMESİ

Nurcan Geçer Ulu

Makine Mühendisliği, Yüksek Lisans

Tez Yöneticisi: Assist. Prof. Dr. Melih Çakmakcı

Ağustos, 2012

Son on yıl içinde, mikro/nano-teknoloji büyük ölçüde gelişti. Mikro/nano-teknoloji ile ilgili ürünler bilim ve teknoloji dünyasındaki uygulamaların yani sira tüketici marketinde de yer almaya başladı. Bu gelişmeler yüksek hassasiyetli pozisyonlama sistemlerine olan ilgiyi arttırdı çünkü yüksek hassasiyetli pozisyonlama sistemleri mikro/nano-teknoloji ile ilgili uygulamalarda cok önemli bi yere sahiptir. Daha kompleks ve ileri düzeydeki uygulamaların daha sıkı toleranslar ve daha küçük parcalar gerektirmesi sonucunda bu beklentileri karşılayabilecek yeni kontrol tekniklerine olan ilgi artmıştır.

Bu çalışmanın amacı yüksek hassasiyetli pozisyonlama sistemlerine yönelik artan ilgiyi karşılayabilecek yeni bir kontrol tekniği geliştirmektir. Bu amaçla, modüler çok eksenli pozisyonlama sisteminin kontrolü çalısılmıştır. Bahsi geçen çok eksenli pozisyonlama sistemi modüler tek eksenli kızakların birleştirilmesiyle oluşturulmuştur. Böylece, tek eksenli pozisyonlama sistemi birkaç şekilde kullanılır ve kullanıldığı alana göre model parametreleri değişir. Bu sebeple, modüler kızakların kullanıldığı alana uyum sağlamaları ve takip hatalarını azaltabilmeleri için tekrarlamalı öğrenme kontrolcüsü geliştirilmiştir. Çok eksenli pozisyonlama sisteminde, kızaklar aynı anda hareket ettirildiğinde birbirleri arasındaki etkileşimler göz önünde bulundurulmalıdır. Bu etkileşimlerin etkisini azaltmak için çapraz bağlaşımlı kontrolcü kullanılabilir ve böylece kontur hatası azaltılabilir.

Bu tezde, takip ve kontur hatasını birlikte azaltmak üzere çapraz bağlaşımlı kontrolcü ve tekrarlamalı öğrenme kontrolcüsünün bir arada kullanıldığı bir kontrolcü geliştirilmiştir. Çapraz bağlaşımlı kontrolcü ile birlikte sunulan kontur tahmin yöntemi yerine işlemsel olarak daha verimli bir kontur tahmin yöntemi kullanılmıştır. Bunun yanında, kullanılan yöntem herhangi bir kontur kontrolü

için ve çok eksenli sistemlerde kullanmak için daha uygundur. Ayrıca, tekrarlamalı öğrenme kontrolcüsünün kullanılması, pratik bir tasarima ve modüler sistemlere uygunluğ arttırmaya yarar. Ayrıca, önerilen kontrolcünün kararlılık ve yakınsama karakteristiği incelenmiştir. Kontrolcünün etkililiği iki ve üç eksenli sistem üzerinde yapılan simulasyon ve deneylerle gösterilmiştir. Sonuçta ortaya çıkan kontrolcü ile nanometre hassasiyetinde takip ve kontur performansı gözlemlenmiştir.

Anahtar sözcükler: Tekrarlamalı öğrenme kontrolü, çapraz bağlaşımlı kontrol, hassas haraket kontrolü.

Acknowledgement

I would like to express my sincere gratitude to my advisor, Assist. Prof. Melih Çakmakçı, for his encouragement, guidance and support throughout my thesis work. His perpetual energy as an advisor and enthusiasm in research had motivated me and made the research period smooth and rewarding.

I would also like to thank all members of Bilkent University Mechanical Engineering Department. Especially, I would like to thank department chair, Prof. Adnan Akay for his support. Moreover, I owe special thanks to Assist. Prof. Sinan Filiz for sharing his experience in precision positioning systems. His help was very important throughout this research. I would also like to express my thanks to Şakir Baytaroğlu for his helpful advice and comments. I would also like to thank undergraduate students working in our lab, Ersun Sozen and Oytun Ugurel.

I would also like to thank my family and friends for their support, love and encouragement.

Above all, I would like to present my deepest thanks to my husband, Erva Ulu.

Contents

List of Figures

List of Tables

Chapter 1

Introduction

Recently, micro/nano-technology has been improved significantly. Micro/nano-technology related products started to be used in consumer market in addition to their applications in the science and technology world. These developments resulted in a growing interest for high precision positioning systems since precision positioning is crucial for micro/nano-technology related applications. For example, multi-axis precision positioning is required in micro/nano-scale manufacturing and assembly, optical component alignment systems, scanning microscopy applications, nano-particle placement applications, cell/tissue engineering and etc.[4, 5, 6]. With the rise of more complex and advanced applications requiring smaller parts and higher precision performance, demand for new control techniques that can meet these expectations is increased.

In an effort to develop a new control technique for high precision positioning systems, control of a modular positioning system is studied in this thesis. The positioning system is modular in the sense that it is constructed by the same single-axis slider to form two-axis and three-axis slider systems. Here, it is aimed to be able to control single-axis, two-axis and three-axis precision positioning systems. In a single-axis precision positioning system, tracking performance is one of the most important factors. For multi-axis systems, high contouring performance is also required. Therefore, in order to achieve high precision positioning, tracking and contouring performance should be considered.

In literature, most of the studies on contour control focus on increasing tracking performance of each axis in order to lead better contour performance. Moreover, some specially designed multi-input-multi-output (MIMO) control algorithms consider the effects between moving axes so that the resulting contour performance is improved. Tracking control algorithms and contour control algorithms can also be used together to achieve higher tracking and contouring performances.

In this thesis, an new method based on cross-coupled control (CCC) and iterative learning control (ILC) which benefits from the contouring error vector approach is presented for multi-axis systems. CCC is a special type of MIMO control that uses contour error as the control parameter whereas ILC is a feed-forward control method that is widely used for tracking control. Since proposed method also benefits from the contouring error estimation vector approach, it is computationally more efficient, more suitable for coupling gain calculations of arbitrary nonlinear contours and easier to implement on multi-axis systems than traditional approaches. Moreover, the presented method utilizes ILC via zero-phase filtering so that the design process for ILC is practical and suitable for modular systems. Since the positioning system is modular, the single-axis stage can be used as x-axis, y-axis or z-axis. Use of iterative learning control also helps modular sliders adapting to repeated disturbances and nonlinearities of the axis they are used for.

Positioning systems, with the increased demand from the industry, are required to have both high precision and high speed operation capabilities in recent years. However, uncontrolled accelerating or decelerating motion causes residual vibrations during high-speed operation. Hence, the accuracy of the system decreases whereas the settling time increases. However, residual vibrations can be prevented by planning the reference trajectory of the system in a way that acceleration and deceleration phases are smoothed out. Although control algorithm presented in this thesis increases contouring and tracking performance, reference trajectory planning is essential for further improvements to achieve high precision. For this purpose, generic s-curve method is employed in this thesis. In this method, position input is designed as an s-shaped curve so that there is no

sudden change in acceleration and velocity during the operation.

The remainder of this thesis is organized as follows. Chapter 2 introduces the modular positioning system used in this thesis with its control setup. Also, the single-axis slider system is examined through its mathematical model considering the assembly configurations. In Chapter 3, tracking control and contour control approaches used in literature are discussed. Chapter 4 presents the learning based cross-coupled controller as well as the cross-coupled controller and iterative learning controller. Stability and convergence of the controller is also analyzed in this section. Effectiveness of the presented control design is verified with simulations and experiments on two-axis and three-axis positioning systems using nonlinear contours in Chapter 5. Simulation and experiment results are supplied for single-axis system control for an s-curved trajectory. Trajectory planning procedure is also explained in this chapter. In Chapter 6, robustness of the control algorithm implementation is tested through some experiments that are designed considering the expected disturbances and system uncertainties. Conclusion and future work is discussed in Chapter 7.

Chapter 2

System Setup and Modeling

This chapter introduces the positioning system used in this thesis with its control setup. Also, the single-axis slider system is examined through its mathematical model development. For this purpose, first, components of the single-axis slider system are explained. Then, control setup is described with the electronic equipment and software used for the control implementation. Whole system with the physical environment is also given as the testbed. Multi-axis configurations of the slider system that are used for the experiments are also provided. To design a controller, mathematical model is an essential requirement. For this reason, a theoretical model of the single-axis slider system is derived and improved by experiments. This section is a revised version of the work given in [7]

2.1 System Setup

Control of single-axis, two-axis and three-axis positioning system is practiced in this thesis. Therefore, system setup includes single-axis and multi-axis (two-axis and three-axis) positioning systems. Moreover, there are other electronicl components and software used for the control of these positioning systems. In order to explain the system setup, single-axis slider system, control setup and multi-axis positioning system are described in this section.
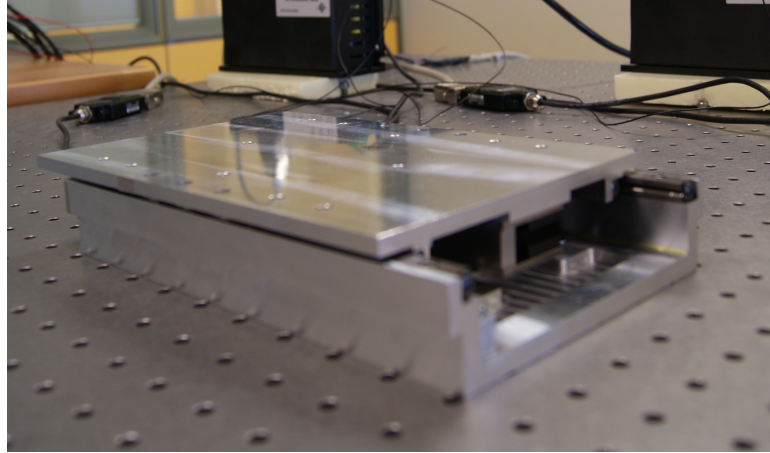
Figure 2.1: Single-axis slider system

2.1.1 Modular Single-Axis Slider System

A modular single-axis stage (Figure 2.1) is composed of a stationary base and a moving slider that are connected to each other via cross-roller linear bearings. The stage is actuated by a brushless permanent magnet linear motor from Aerotech Inc. whereas the position feedback is taken from an incremental linear encoder from Heidenhain Corp. Since position is measured directly on the stage with a linear encoder, positioning becomes extremely reliable. The linear encoder has an optical scale with four micrometer in pitch leading one micrometer resolution. However for our system, the encoder resolution is increased to 25 nm using an interpolation technique. Details of interpolation procedure can be found in [8]. Travel range of the stage is 120mm and the maximum encoder traversing speed that is 500mm/s limits velocity of the system.

2.1.2 Control Setup and Testbed

In addition to the positioning system, electronic hardware and software is used for the control of the system. First a control panel should be developed to give inputs to the system and implement the developed control architecture. For this purpose, Labview software is used on a PC. The control signal is transferred to the

5
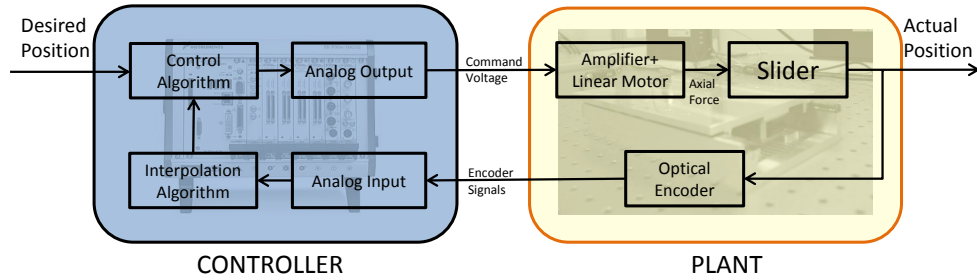
Figure 2.2: Closed loop control setup of the single-axis system

amplifier by data acquisition system. Then, a standard current commanded six-point commutation amplifier is used for commutation of three phases of the linear motor. The position feedback is taken from the encoder by the data acquisition system. Closed loop configuration of the control setup for single-axis stage is given in Figure 2.2.

For precision positioning systems, small disturbances can deteriorate the performance significantly. Due to this fact, elimination of disturbances is very important. One of the most important disturbance type may be the environmental vibration. In order to minimize environmental vibration, the modular stage is mounted on a vibration isolation table. Figure 2.3 shows the photograph of testbed for the single-axis slider system.

2.1.3 Multi-Axis Positioning System

In this thesis, two-axis and three-axis positioning system control is studied for multi-axis position control. The two-axis positioning system is constructed by assembling two modular single-axis stages perpendicularly as in Figure 2.4. In three-axis positioning system, a vertical axis is used in addition to two horizontal axes (Figure 2.5). In order to assemble vertical axis, an adapter is used. This adapter part is composed of an L-beam and a counterbalance system that is used for the compensation of vertical sliding mass.

6

Figure 2.3: Photograph of testbed for the single-axis slider system

2.2 Modeling

Mathematical model is crucial for simulation studies and theoretical analysis. In this section, mathematical model of a single-axis slider is derived. Then, the mathematical model is improved by experiments to achieve matching responses for simulations and experiments.

2.2.1 Mathematical Model of The Modular Single-Axis Slider System

The slider system is composed of two main components as the fixed base and the sliding part. Figure 2.6 presents the sliding part of the single-axis slider system. This part is composed of aluminium top, motor track, encoder scale and one side of the bearings. The only contact mechanism in the sliding part is the linear cross-roller bearings. Moreover, the actuating force comes from motor track. These forces are shown in Figure 2.6.
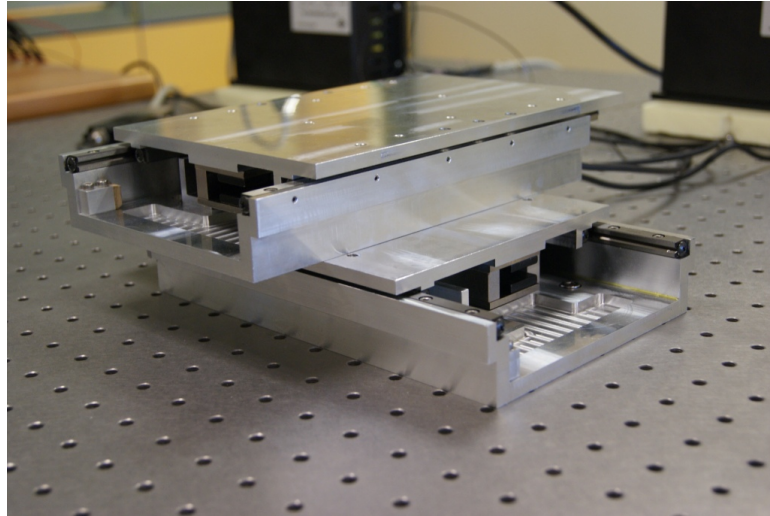
Figure 2.4: Two-axis positioning system
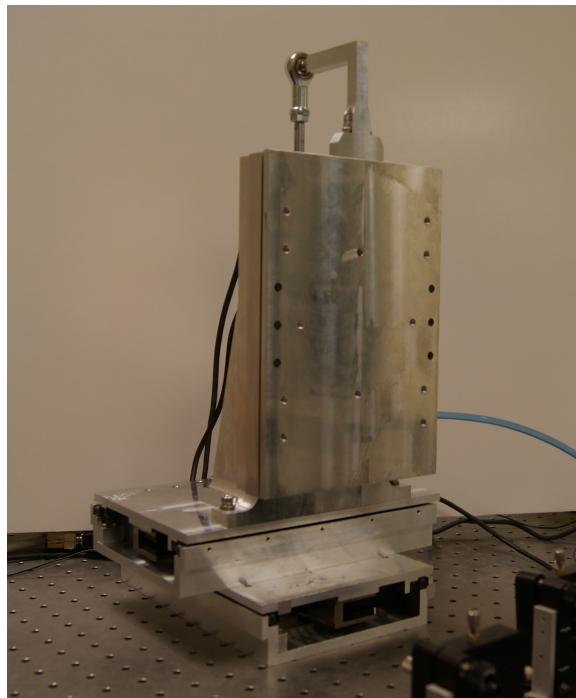
Figure 2.5: Three-axis positioning system
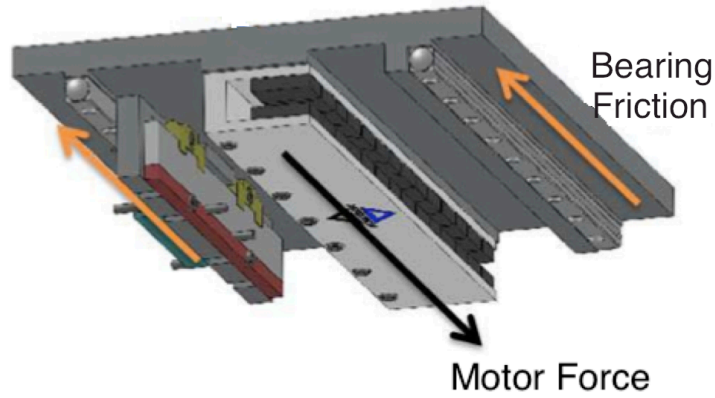
Figure 2.6: Forces acting on the moving slider

As mentioned in the previous sections, single-axis slider system can be used in both horizontal and vertical configurations. Therefore, both configurations should be considered for the mathematical model. In Figure 2.7, forces acting on the sliding mass in the direction of movement is given for both horizontal and vertical configurations of the slider. In the free body diagram, linear bearings are modeled as part of the viscous friction component. Moreover, force ripple in the linear motor is neglected. Since use of counter balance aims to compensate weight of the sliding mass. counter balance force, f_c is equal to the weight of the sliding mass, mg. When these two forces cancel each other, horizontal and vertical free body diagrams are equivalent. Therefore, both configurations of the sliding mass can be modeled through same equations.

Idealized dynamic model of a single-axes linear stage is given in Figure 2.8 where R is linear motor resistance, L is linear motor inductance, K_{BEMF} is back electromotive constant, K_{force} is force constant, m is sliding mass, b is viscous friction, e is linear motor input voltage, K_{amp} is amplifier gain and i is linear motor current. In the dynamic model, ripple forces of the permanent magnet linear motor are neglected and linear bearings are modeled as viscous friction component as in free body diagram.
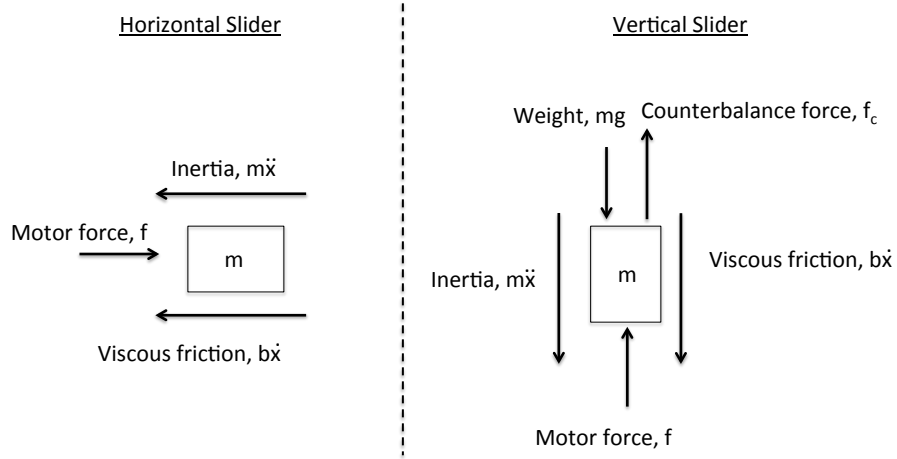
Figure 2.7: Free body diagram of the moving slider
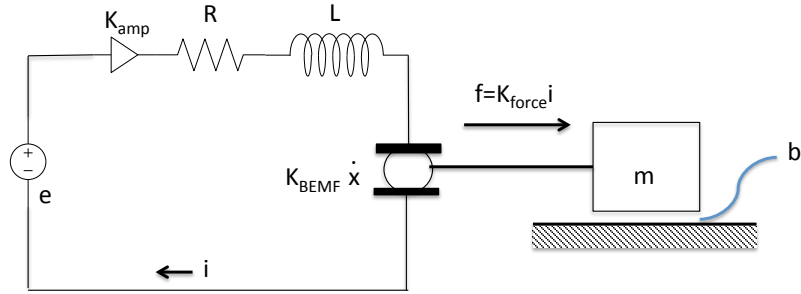
Figure 2.8: Dynamic model of the single-axis system

Using Newton's law of motion, equation of motion for the sliding part can be given as

$$f(t) - b\dot{x}(t) - m\ddot{x}(t) = 0 \tag{2.1}$$

Dynamic equations of the permanent magnet linear motos are found as

$$e(t) = K_{amp}(Ri(t) + L\dot{i}(t) - K_{BEMF}\ddot{i}(t)) \tag{2.2}$$

$$f(t) = K_{force}i(t) \tag{2.3}$$

10

Taking Laplace transform of (2.1), (2.2), (2.3) and arranging, plant transfer function from input voltage e to slider displacement x is found as in (2.4). Block diagram of the single-axis slider plant, P, is given in Figure2.9.

$$P(s) = \frac{X(s)}{E(s)}$$
$$= \frac{K_{amp}K_{force}}{s[Lms^2 + (Rm + bL)s + (Rb + K_{BEMF}K_{force})]}$$

(2.4)
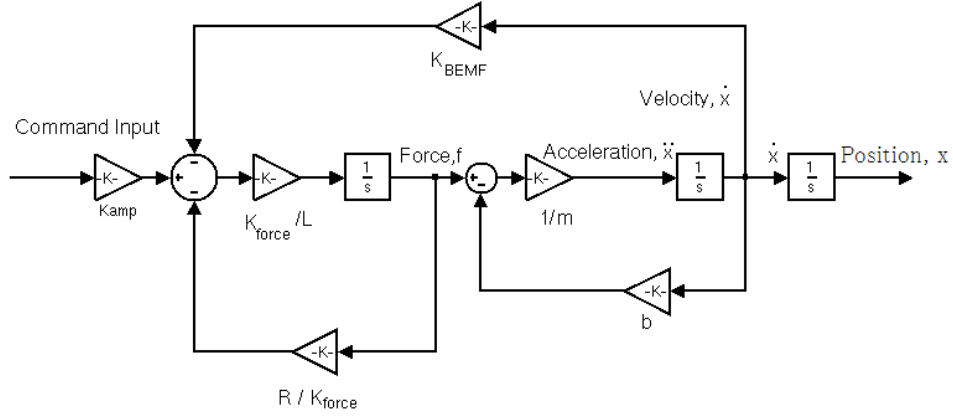
Figure 2.9: Block diagram of the mathematical model

2.2.2 Model Improvement Tests

In the transfer function of the plant, viscous friction, and amplifier gain is unknown. Hence, series of experiments are conducted to obtain a numerical expression for the transfer function between input voltage, e, and slider displacement, x. For this purpose, plant transfer function of single-axis slider system is approximated by

$$P(s) = \frac{X(s)}{E(s)} = \frac{G_{DC}\omega_n^2}{s(s^2 + 2\zeta\omega_n s + \omega_n^2)}e^{-s\tau}$$

(2.5)

where G_{DC} is DC gain, ζ is damping ratio, ω_n is natural frequency, and τ is time delay.

11

In order to find DC gain, open loop steady state step response of the plant can be used. However, when constant step input is send to open loop plant, position response gives a ramp like output due to the free integrator in the transfer funkiction. Yet, velocity response may reach a steady state value. Since velocity is simply time derivative of displacement, the transfer function between the control input and velocity can given as in (2.6). In the equation, $V(s)$ represent the laplace transform of velocity, $\dot{x}(t)$.

$$P_v(s) = \frac{V(s)}{E(s)} = \frac{G_{DC}\omega_n^2}{s^2 + 2\zeta\omega_n s + \omega_n^2} e^{-s\tau} \tag{2.6}$$

A step input with magnitude, a, is applied to the system. Laplace transform of a step input with magnitude, a, is

$$E(s) = \frac{a}{s} \tag{2.7}$$

Then, the step response is found as in (2.8). Steady state value of the velocity response is derived by taking limit of the step resonse. When $t \to \infty$, $s \to 0$. Therefore, steady state value for velocity response, v_{ss}, becomes (2.9). Using (2.9), the relation to calculate DC gain is obtained as (2.10)

$$V(s) = E(s).P_v(s) = \frac{aG_{DC}\omega_n^2}{s^2(s^2 + 2\zeta\omega_n s + \omega_n^2)} e^{-s\tau} \tag{2.8}$$

$$v_{ss} = \lim_{s \to 0} V(s) = \lim_{s \to 0} \frac{aG_{DC}\omega_n^2}{s^2(s^2 + 2\zeta\omega_n s + \omega_n^2)} e^{-s\tau} = a.G_{DC} \tag{2.9}$$

$$G_{DC} = \frac{v_{ss}}{a} \tag{2.10}$$

Velocity response of the plant for step input with magnitude of $0.49V$ is fiven in Figure 2.10. As can be observed from the figure, steady state value of velocity is about $150-155mm/s$. Considering these values, DC gain is taken as $318mm.V/s$. In the experiments, magnitude of the control input is critical because slider does not even move under $0.49V$ and velocity can not reach a steady state value before

track is finished when the control input is higher. Due to this fact, velocity response could not be provided for a longer range of motion in Figure 2.10.
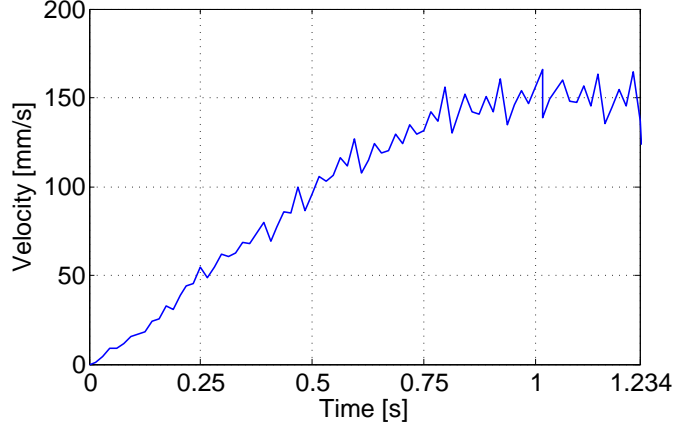
Figure 2.10: Velocity step response

For gross estimates of ζ and ω_n, velocity impulse response characteristics are examined through series of experiments. The obtained velocity impulse response is fitted to the time solutions for the impulse response, $c(t)$, for over-damped ($\zeta > 1$) systems given in [9] as

$$c(t) = \frac{\omega_n}{2\sqrt{\zeta^2 - 1}}e^{-(\zeta - \sqrt{\zeta^2 - 1})\omega_n t} - \frac{\omega_n}{2\sqrt{\zeta^2 - 1}}e^{-(\zeta + \sqrt{\zeta^2 - 1})\omega_n t} \; for \; t \geq 0 \quad (2.11)$$

so that the system characteristics ζ and ω_n are obtained as $1.1rad/s$ and $150rad/s$. On the other hand, τ can be estimated as $0.015s$ by observing the closed loop step response for position loop and the controller output.

In order to compare the simulation and experimental results of the model, a PID controller is designed. Structure of the controller is

$$G_c(s) = K_c(1 + \frac{1}{T_i s} + T_d s) \quad (2.12)$$

where K_c, T_i and T_d are proportional gain, integral time and derivative time,

13

respectively. In order to design the PID controller, $G_c(s)$, the design objective is chosen so that the closed loop transfer function is

$$\frac{G_c(s)P(s)}{1 + G_c(s)P(s)} = \frac{1}{1 + sT_\alpha} \tag{2.13}$$

where T_α is the desired time constant of the closed loop response. Following the work given in [3], PID controller parameters can be chosen as

$$K_c = \frac{1}{G_{DC}T_dT_\alpha\omega_n^2} \quad T_i = \frac{2\zeta}{\omega_n} \quad T_d = \frac{1}{\omega_n^2 T_i} \tag{2.14}$$
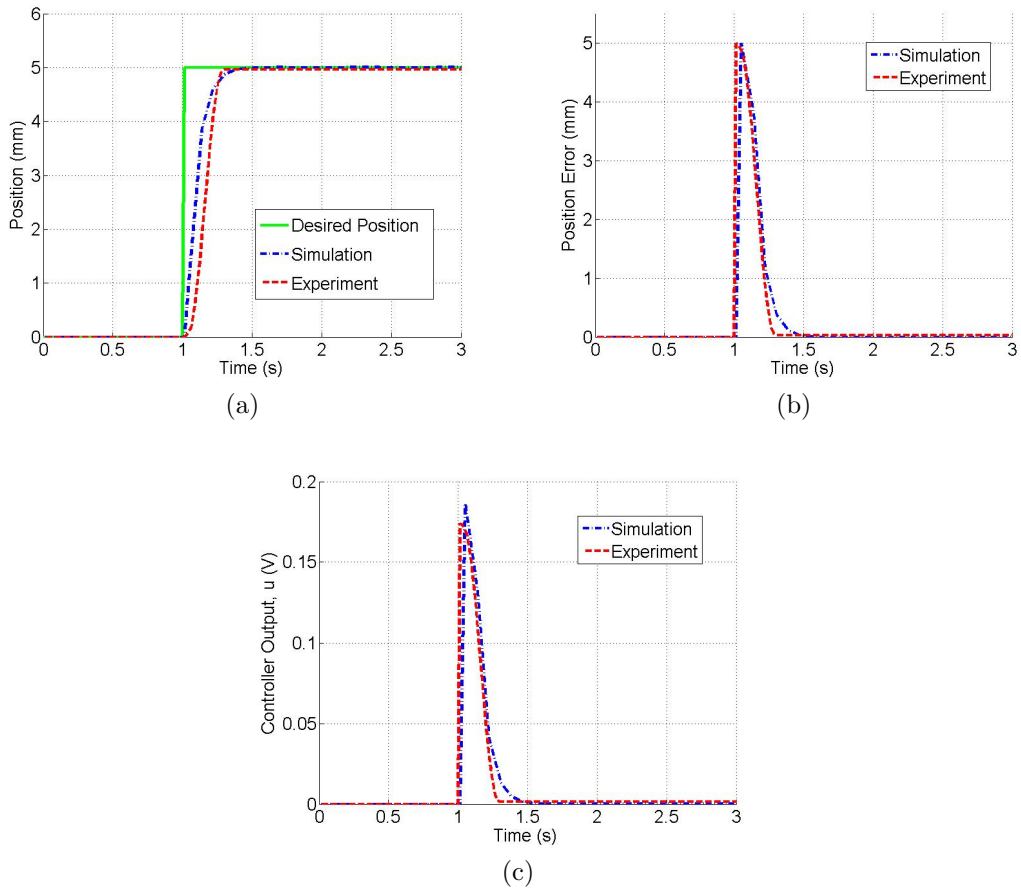
Figure 2.11: Step response characteristics comparison for (a) Position, (b) Position Error and (c) Controller Output

Choosing a suitable T_α, PID controller parameters are obtained using (2.14). However, these parameters give a step response with undesirable overshoot in the simulation. Hence, by fine tuning, a new set of PID controllers are obtained so that the system shows over-damped step response characteristics both in simulation and experiment as shown in Figure 2.11. The system behavior with these controller parameters are similar for simulation and experiment proving that the mathematical model estimation is well enough to describe the system.

Chapter 3

Literature Survey

Recently, micro/nano-technology has been improved significantly. Micro/nano-technology related products started to be used in consumer market in addition to their applications in the science and technology world. These developments resulted in a growing interest for high precision positioning systems since precision positioning is crucial for micro/nano-technology related applications. With the rise of more complex and advanced applications requiring smaller parts and higher precision performance, demand for new control techniques that can meet these expectations is increased.

In an effort to develop a new control technique for high precision positioning systems, control of a modular positioning system is studied in this thesis. The positioning system is modular in the sense that it is constructed by the same single-axis slider to form two-axis and three-axis slider systems. Here, it is aimed to be able to control single-axis, two-axis and three-axis precision positioning systems. In a single-axis precision positioning system, tracking performance is one of the most important factors. For multi-axis systems, high contouring performance is also required. Therefore, in order to achieve high precision positioning control, tracking and contouring performance should be considered. Next two sections will describe tracking control and contour control approaches used in literature.
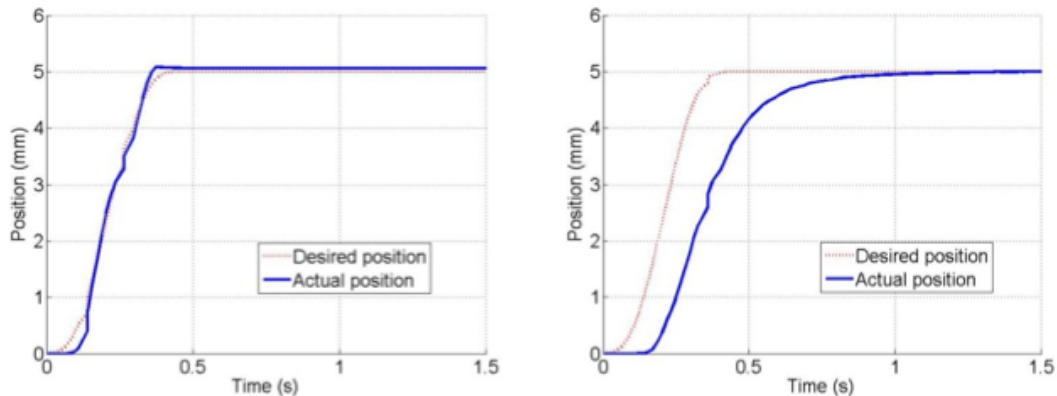
Figure 3.1: Trajectory tracking

3.1 Tracking Control

In tracking control, the objective is moving along a desired trajectory. In Figure 3.1, an example trajectory tracking is given. In the figure, the left plot shows a better tracking response compared to the one at the right since most of the actual movement is along the desired trajectory. Most commonly used tracking control method is feedback control with PID [10, 5, 11, 12, 13]. Sliding mode controller is also used as a feedback tracking control in [14, 15]. Almost all systems employ feedback as a part of tracking control however substantial improvement of tracking accuracy is achieved by addition of feed-forward control. Several feed-forward control schemes developed to improve tracking accuracy in literature such as zero phase error tracking control (ZPETC) [16, 17, 18], feed-forward friction compensation [19, 14, 20] and iterative learning control (ILC) [3, 21].

Tracking performance of a ZPETC system is sensitive to variations in plant parameters and modeling errors since ZPETC design is based on pole/zero cancellation and phase cancellation [16]. Friction compensation techniques generally incorporate a system identification process that should be repeated if system parameters change. Tan et al. [3] claims that specifying a plant model for ILC via zero phase filtering is not necessary due to the principle of self-support that is argued in [22]. Since the stored control signals reflect the plant characteristics, ILC can improve tracking performance of a system even the plant structure and

nonlinearities are unknown [23]. However, the system should execute the same task repetitively to be able to implement an ILC scheme.

Iterative learning control can be applied to the systems that repeatedly execute the same operation. By applying it, experience gained from the repeated execution is used to improve the performance of the system. Considering this fact, iterative learning control schemes are suitable to be used in high precision control of linear motors. In the literature, there are a several cases in which various iterative learning control schemes are applied in combination with some other control techniques for linear motor control purposes. In [24], frequency based ILC, H_∞ based ILC and second order ILC approaches are considered for linear motor motion system. Scholten simulated these three alternatives and compared their performance. As a result Scholten concluded that the best performance is achieved by second order ILC although all of the ILC types improved the performance of the system with conventional control schemes. In all cases, Scholten claims that the tracking error is decreased compared to the ones with the conventional controllers. In [25], internal model based iterative learning control for linear motor motion systems are considered. According to Fan et al., the main reason for linear motor not to reach high tracking accuracy is nonlinear disturbances. In order to achieve high tracking accuracy by rejecting the nonlinear disturbances, they combine the iterative learning control with internal model control. Hence, they claim that ILC based on internal model control can guarantee the robust performance and high tracking accuracy with the experience obtained from early stages of learning.

Linear parameter varying iterative learning control for linear motor systems is explained in [26]. In this paper, the basic assumption is that the dynamics of the system change between iterations. According to Butcher et al., permanent magnet linear motors are affected by periodic, position dependent force disturbance. Although these periodic disturbances can be eliminated by using ILC, if the initial position of the system changes, the disturbance changes so that learned input will not lead to the optimal tracking. For this reason, they proposed linear parameter varying ILC for linear motor control purposes. As a result of their work, it is claimed that better results are obtained using the proposed method compared to

18

the one using linear time invariant ILC. Another research on iterative learning based control of linear motor is given in [3]. They combined relay tuning and ILC based on zero-phase filtering to control high precision linear motor in their work. Tan et al. improves the tracking performance of the linear motor by applying ILC based zero-phase filtering as feedforward controller to the relay tuned PID feedback controller. As a result of experiments, the proposed method in their work has higher effectiveness to be used in linear motor control purposes.

3.2   Contouring Control
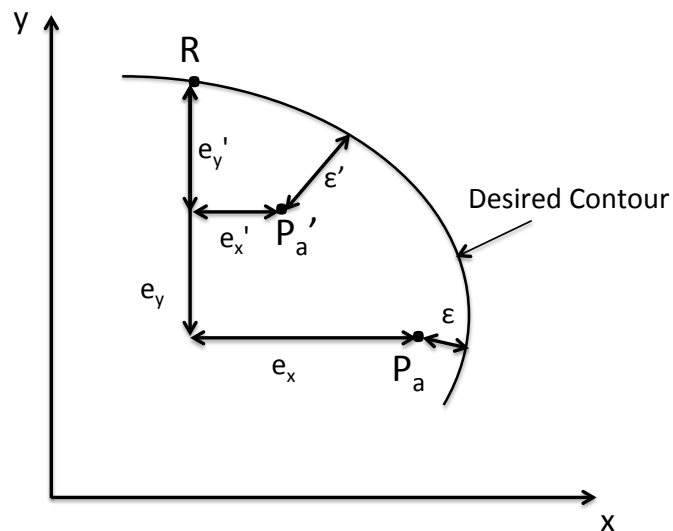
Figure 3.2: Tracking and contour error

In literature and commercial products, contouring control is achieved by improving tracking of the systems. Generally, improving tracking accuracy of an individual axis also increases contouring accuracy of the multi-axis system. However, reducing tracking error does not necessarily result in a reduction in contour error in nonlinear cuts [27]. In some cases, decreasing the tracking error may not decrease the contour error; it may even deteriorate the contouring performance. This can be observed in Figure 3.2. The axial errors are defined as the distance between the desired position, R and the actual position, P_a. Contour error, ε, is defined as the distance between actual position and nearest position on the

desired contour as shown in Figure 3.2. When the actual position is moved to P'_a from P_a decreasing the axial tracking errors from e_x and e_y to e'_x and e'_y, contour error, ε increases and becomes ε'. Therefore, special control approaches should be employed for contour control since in contouring applications contour tracking is more important then trajectory tracking.

For contouring control, first the system should have a good tracking control in each single-axis. Then, contour control can be accomplished through different MIMO control schemes. Koren [28] proposed the cross-coupled control (CCC) structure that focuses on eliminating the error in contouring rather than tracking in individual axes, This method is proven to reduce contour error significantly. Since the introduction of CCC, many controllers based on CCC has been developed. Other than CCC and its modified versions, model predictive contour control for biaxial feed drive systems is presented in [2]. Next subsections describe model predictive contouring control and CCC and CCC based contouring controls. Then, contour error models are discussed.

3.2.1   Cross-coupled Control

For contour control, Koren proposed cross-coupled control (CCC), which is the first control scheme to consider mutual dynamic effect among all axes, in [9]. Cross-coupled control scheme introduced the notion of finding the contour error from multiple error signals, applying some form of control to the combined signal, and feeding the new signal back into the respective systems. This concept is a special type of multi input multi output (MIMO) control which aims to decrease the contour error. Block diagram of this control scheme is given in Figure3.3. In the block diagram, C_x and C_y are coupling gains whereas ε, e_x, e_y are the contour error, x-axis tracking error and y-axis tracking error respectively. As can be observed form Figure3.3, contour error is obtained through (3.1)

$$\varepsilon = -C_x e_x + C_y e_y \qquad (3.1)$$
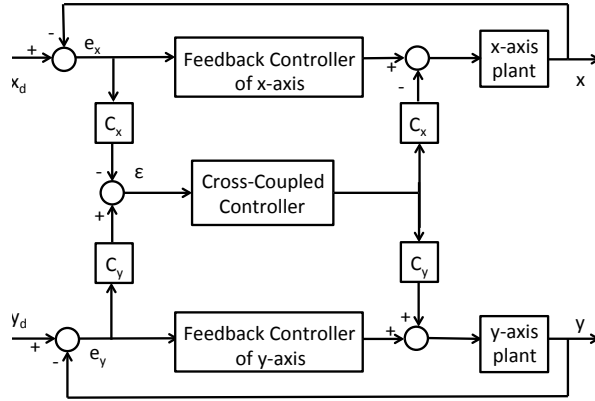
Figure 3.3: Block Diagram of CCC

Although CCC is first introduced with constant gains in [28], the term CCC is generally used for CCC with variable coupling gains as proposed in [27]. The next section describes the proposed modifications and combnations of CCC.

3.2.2 Variations and Combinations of CCC

Since the introduction of CCC, it has been modified and combined with different control techniques. In this section development of CCC to its form that is used today will be outlined. Then, other control designs integrating another control schemes to CCC are examined.

First, Koren introduced CCC around 1980s [28]. This method was the first approach to use a specific controller for contour control instead of improving tracking accuracy only. In this approach, contour error is acquired by combining axial error signals and feeding the new signal back into the respective systems after applying some control. Then, this work was followed by several papers from Kulkarni and Srinivasan [29, 30, 31, 32]. Srinivasan and Kulkarni came out with a new CCC design which separated the contour error into two different signals for the x and y axis respectively in 1990 [33]. After this design, Koren introduced the variable-gain cross-coupling controller which is currently the most widely used design in industry [27]. Recently, widely used CCC method is also adapted as in
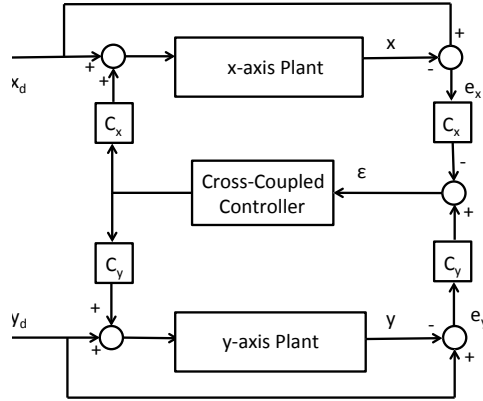
Figure 3.4: Block Diagram of Position Based CCC

Figure 3.4. This position based configuration of CCC is proposed in [34].

Tracking control and contour control are two essential parts of contouring. In the literature, control schemes for tracking and contour control are combined in various ways to improve contouring. Some examples can be given as observer-based CCC [35], cross-coupled model reference adaptive control[36], cross-coupled iterative learning control (CCILC) [21], CCC with disturbance observer and ZPETC [18], CCC with friction compensation [14] and CCC with ILC [21, 37, 38].

3.2.3 Contour Error Estimation Models

Since CCC based control schemes require contour error as the control parameter, there is a need for a contour error model in real time. Contour error is defined as the distance between actual position and nearest position on the contour [1]. Contour error can be calculated easily for linear contours. However, this calculation is very complicated for nonlinear contours, especially during the operation. Hence, some approximations have been used to calculate a nonlinear contour error. The most common one is using the circular contour assumption suggested by Koren et al. [27]. Yeh and Hsu [1] proposed another method that approximates contour error as the vector from the actual position to the nearest point on the line that passes through the reference position tangentially. The latter approach

has several advantages over the former as computational efficiency, suitability for arbitrary contours and convenience for multi-axis implementation [1]. Recently, an iterative approach is develop to improve estimated contour error in [39]. For the estimation of contour error, there are two basic models circular contour approach and tangential contour error approximation. Next two parts will briefly present these approximations.

3.2.3.1 Circular Contour Assumption

In this approach any arbitrary contour is separated into parts with radius of curvature ρ and these parts are approximated by circles. Since contour error for a circular contour is the difference between the distance from the actual position to the center of the circle and radius of the circle, contour error for an arbitrary contour can be written as (3.2)

$$\varepsilon = \sqrt{(x - x_0)^2 + (y - y_0)^2} - \rho \tag{3.2}$$

where (x_0, y_0) and (x, y) denote center of the curvature and actual position, respectively. Expressing the actual position with respect to reference position and axial tracking errors, e_x, e_y and using Taylor expansion, approximated contour error becomes (3.3)

$$\varepsilon = (\cos\theta + \frac{e_y}{2\rho})e_y - (\sin\theta - \frac{e_x}{2\rho})e_x \tag{3.3}$$

where θ is traversal angle of motion and ρ is the radius of curvature at the point. In (3.3), ρ is infinity for linear contours. Moreover, ρ becomes the constant radius of circle for circular contours.
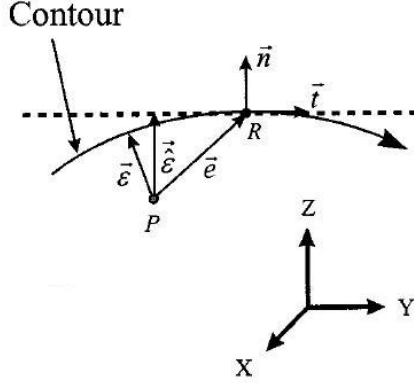
Figure 3.5: Geometrical Relations of Contour Error (adopted from[1])

3.2.3.2 Contouring Error Vector Approach

Contour error vector approach can be explained through the geometrical relations in the multi-axis motion control system given in Figure3.5. In the figure, $\overrightarrow{e}$ is tracking error vector, $\overrightarrow{\hat{\varepsilon}}$ is estimated contour error vector, $\overrightarrow{\varepsilon}$ is contour error vector, $\overrightarrow{t}$ is normalized tangential vector, $\overrightarrow{n}$ is normalized normal vector, P is actual position and R is reference position. In this approach, contouring error $\overrightarrow{\varepsilon}$ is defined as the vector from the actual position to the nearest point on the line that passes through the reference position tangentially with direction $\overrightarrow{t}$ [1]. This approach estimates contour error vector very closely when tracking error is small enough. Looking at Figure3.5, $\overrightarrow{\hat{\varepsilon}}$ is equal to $\langle \overrightarrow{e}, \overrightarrow{n} \rangle$ where $\langle .,. \rangle$ is inner product operator. Hence, relation between $\overrightarrow{\hat{\varepsilon}}$ and $\overrightarrow{e}$ can be obtained using inner product. Furthermore, the contour error is calculated as $|\overrightarrow{\hat{\varepsilon}}| = \sum_i C_i e_i (i = x, y, z)$ where C_i is coupling gain and e_i is the corresponding axial tracking error. Considering these two representations of estimated contour error vector, cross coupling gains (C_x, C_y, C_z) in terms of normalized normal vector $(\overrightarrow{n} = [n_x\ n_y\ n_z]^T)$ are found as $C_i = n_i (i = x, y, z,)$. In other words, cross coupling gains at a point are the elements of unit normal vector of the contour at that point.

24

3.2.4　Model Predictive Contouring Control

This control method uses model predictive control strategy that utilizes an explicit process model and tracking error dynamics to predict the future behavior of a plant. Model predictive contouring control delivers a novel approach towards improving contour accuracy. As mentioned in previous section, contour error can be estimated as the vector from the actual position to the nearest point on the line that passes through the reference position tangentially. Considering this the error components orthogonal to the desired contour curves are more important than tracking errors, and hence, control inputs are found from the normal and tangential components of the axial errors.
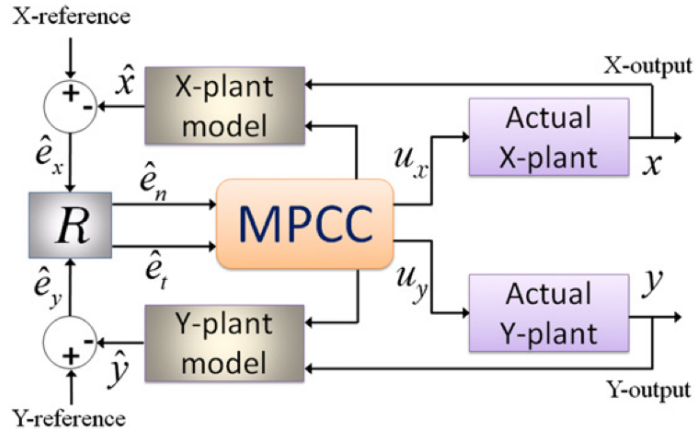
Figure 3.6: Model Predictive Contouring Control Diagram [2]

Block diagram of the proposed contouring control system is as in Figure 3.6. In the MPCC box, a minimization problem given in (3.4) is solved. ρ_{cn} and ρ_{ct} are weighting factors to adjust the importance of the error component in the orthogonal and tangential directions, respectively, ρ_n and ρ_t are weighting factors used to adjust the control inputs in the normal and tangential directions, respectively, and u_{xj} ; u_{yj} ; u_{nj} and u_{tj} are the jth control inputs in the x, y, n and t directions, respectively, H_M and H_p defines the prediction horizon.

$$J = \rho_{cn} \sum_{j=H_M}^{H_p} e_{n_j}{}^2 + \rho_{ct} \sum_{j=H_M}^{H_p} e_{t_j}{}^2 + \rho_n \sum_{j=H_M}^{H_p} u_{n_j}{}^2 + \rho_{cn} \sum_{j=H_M}^{H_p} u_{t_j}{}^2 \qquad (3.4)$$

3.3 Conclusion

To sum up, tracking control and contour control are two essential parts of contouring. In the literature, control schemes for tracking and contour control are combined in various ways to improve contouring. Model predictive contouring control method provides an efficient contour control. However, cross-coupled control has been used for this purpose for a longer time and effectiveness of this method is proven by many researchers. Moreover, model predictive contouring control is only used for biaxial systems although it is claimed that the controller can be extend to multi-axis systems. In this thesis, developed controller should work on multi-axis systems that can be have more than two axes. Moreover, using ILC is beneficial for our system since it is modular. The slider system can be used for many positions, being able to improve its tracking is an advantage of ILC when position of the modular slider is changed. This way, system can show good performance even its position is changed or any other slider is assembled on it.

For contour error estimation models, although two described approaches give similar results in terms of contouring accuracy, contour error vector method has several advantages over the circular contour assumption. Firstly, it is computationally more efficient. An extensive study on the computational efficiency of the contour error vector approach over the circular contour approach is given in [1]. Moreover, with contour error approach, coupling gains can be computed easier for an arbitrary contour. Also, implementation of contour error vector approach to multi-axis systems is accomplished by the same procedure used for two-axis systems and this procedure is well established. Therefore, contour error vector approach is more suitable for multi-axis systems.

Chapter 4

Development of The Control Algorithm

The multi-axis precision positioning system is constructed by assembling modular single-axis stages. The single-axis stage is modular in the sense that couple of them can be assembled together to form two or three-axis positioning systems. Therefore, a single-axis stage can be used as x-axis, y-axis or z-axis. Model parameters of a single-axis stage change depending on which axis it is used for. For this reason, an iterative learning controller is designed to improve tracking performance of a modular single-axis stage after a feedback controller is found as explained in Chapter 2. Use of iterative learning control also helps modular sliders adapting to repeated disturbances and nonlinearities of the axis they are used for.

In this chapter, an new method based on CCC and ILC which benefits from the contouring error vector approach is presented. A preliminary study for using CCC and ILC together is given in [38]. Also, Barton et al. worked on controllers incorporating CCC and ILC for contours combining lines and circles on a two-axis system in [21, 37]. As one of the main contributions, proposed method also benefits from the contouring error estimation vector approach. The method presented here is computationally more efficient, more suitable for coupling gain

calculations of arbitrary nonlinear contours and easier to implement on multi-axis systems than traditional approaches. Moreover, our method utilizes ILC via zero-phase filtering so that the design process for ILC is practical and suitable for modular systems. Other important contribution of the method is that this is the first time CCC and ILC is used together to achieve nanometer level precision. Moreover, the controller is not only designed for two-axis systems but also multi-axis systems (two or more).

Here, an extended study on our work presented in [40] is given. Next section describes zero filtering based ILC. Cross-coupled control implementation is discussed in the second section. Then, the proposed learning based cross-coupled controller is explained. Stability and convergence of the controller is examined in the last section. Effectiveness of the control design is verified with simulations and experiments on two-axis and three-axis positioning systems using nonlinear contours. Simulation and experiment results are provided in Chapter 5.
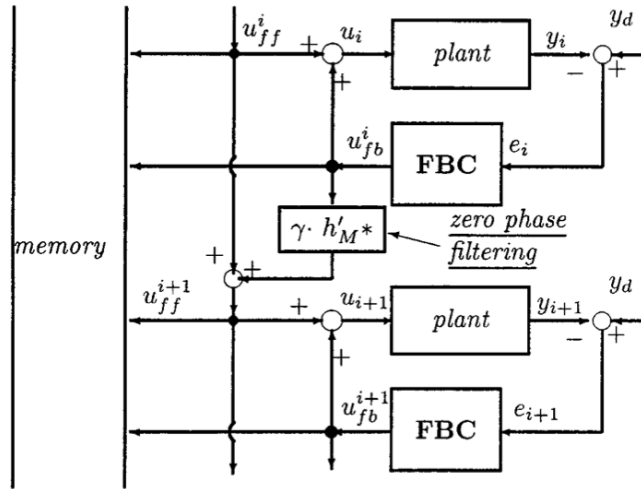
Figure 4.1: Block Diagram of ILC via Zero-Phase Filtering with Feedback Controller [3]

4.1 Iterative Learning Controller via Zero-phase Filtering

ILC is a technique for improving the transient response of a system that operates repetitively. ILC can often be used to achieve perfect tracking, even when the model is uncertain or unknown and there is no information about the system structure and nonlinearity [23]. ILC based on zero phase filtering is a practical and efficient implementation of ILC [3].
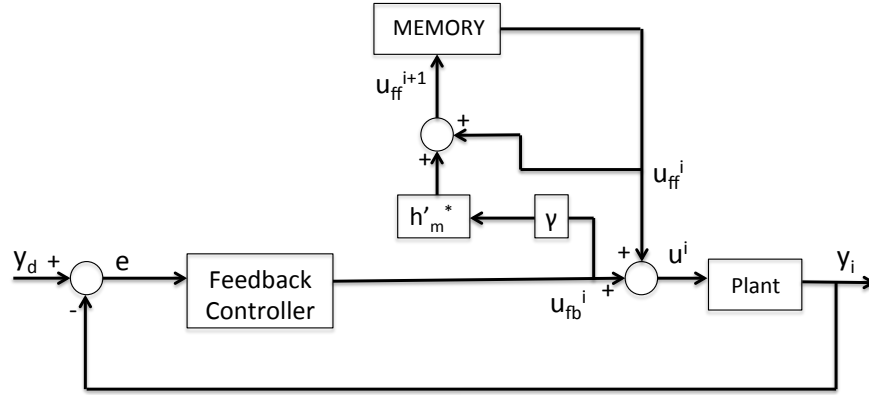
Figure 4.2: Reorganized Block Diagram of ILC via Zero-Phase Filtering with Feedback Controller

Block diagram of zero-phase filter based iterative learning controller is given as Figure 4.1 in [3]. In Figure 4.2, a reorganized version of this control scheme is provided to see it in a traditional block diagram form. In both diagrams, superscript i is iteration number whereas u_{ff}^i, u_{fb}^i and y^i are feed forward control signal, feedback control signal and system output at i^{th} iteration. Moreover, y_d is the desired system output which does not change between iterations. h'_m* is algebraic averager and γ is learning gain. The feed forward control signal for i^{th} iteration is calculated using the feed forward and feedback control signals of the previous iteration that are shown as u_{ff}^{i-1} and u_{fb}^{i-1} respectively. The learning update law can be given as in (4.1)[3].

$$u_{ff}^i(k) = u_{ff}^{i-1}(k) + \frac{\gamma}{2M+1} \sum_{j=-M}^{M} u_{fb}^{i-1}(k+j) \tag{4.1}$$

where k is the time index, γ is the learning gain and M is the length index of zero phase filter. Detailed guidelines for the design of parameters γ and M can be found in [3]. For our system, M is used as 11 and γ is taken as 0.2. Although choosing suitable M and γ values is crucial for convergence, a suitable set of M and γ values can be used for many processes. For example, the same M and γ values are used in all our single-axis, two-axis, three-axis simulations and experiments. In the Simulink implementation, first the block diagram is executed, then a learning m.file is executed for each iteration. The learning m.file is the implementation of (4.1). Simulink block diagrams and real-time Labview VI's and front panels of single-axis ILC implementation are given in Appendix A and B, respectively.

4.2 Cross-coupled Control with Contouring Error Vector Approach
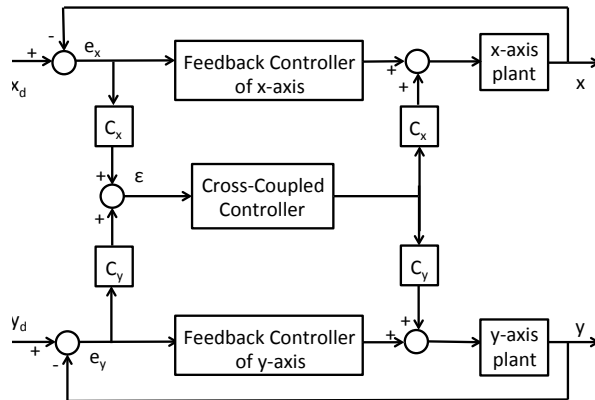
Figure 4.3: Block Diagram of Cross-coupled Control with Contouring Error Vector Approach

Cross-coupled controller is designed in order to consider the effects between axes. Contouring error vector approach is used to calculate the coupling gains

of the cross-coupled controller. Block diagram of the cross-coupled controller is given in Figure 4.3.In the block diagram, C_x and C_y are coupling gains whereas ε, e_x, e_y are the contour error, x-axis tracking error and y-axis tracking error respectively.
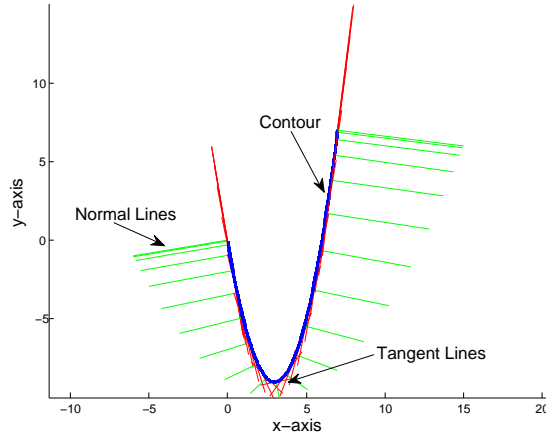
Figure 4.4: 2D contour with its tangents and normals

In contouring error vector approach, contouring error $\overrightarrow{\varepsilon}$ is defined as the vector from the actual position to the nearest point on the line that passes through the reference position tangentially with direction $\overrightarrow{t}$ [1]. Cross coupling gains at a point are calculated as the elements of unit normal vector of the contour at that point. Therefore, cross-coupling gains are

$$C_i = n_i \qquad (i = x, y, z,) \tag{4.2}$$

where (C_x, C_y, C_z) are coupling gains and $(\overrightarrow{n} = [n_x \ n_y \ n_z]^T)$ is the unit normal vector. For the control implementation, coupling gains are found through the developed coupling gain m.file. To find the coupling gains, normals of the contour at each reference point is found. In Figure 4.4, a two dimensional contour is shown with its tangents and normals at some reference points. Components of the unit normal vector at a reference point gives the coupling gains.

31
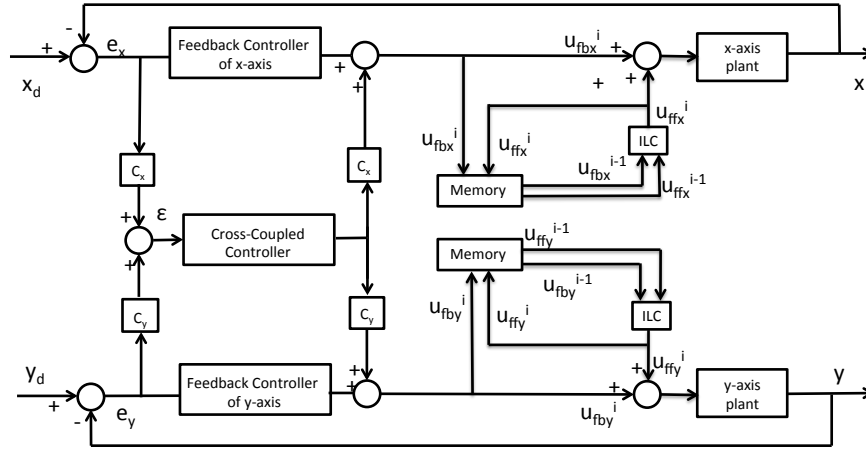
Figure 4.5: Learning Based Cross-coupled Controller for Two-axis Systems

4.3   Learning Based Cross-coupled Controller

The control system is intended to be modular considering being able to inter-change the stages without changing the control system. For modularity concerns, ILC is chosen for improving tracking performance since controller structure does not change with changes in plant model structure and parameters. Moreover, use of ILC is beneficial for modular systems to compensate for changes after the assembly. For example, when a modular stage is assembled on top of another, weight of the sliding mass changes. Since there are only two design parameters in single-axis control scheme of ILC via zero-phase filtering, the implementation is practical. Moreover, contouring error vector method is chosen to use with CCC since it is computationally more efficient. As mentioned before, encoders of the positioning system have been interpolated to achieve nanometer resolution. This procedure is accomplished without any extra hardware. Due to this fact, there is a trade of between resolution of the encoders and the computational effort in the control loop. Therefore, it is aimed to minimize computational effort in the control loop to maximize encoder resolution. Using contouring error vector technique also makes the control method more suitable to implement on multi-axis systems and to operate with arbitrary nonlinear contours. To sum up, a control method featuring CCC and ILC via zero phase filtering has been developed incorporating the contouring error vector estimation technique (Figure 4.5).
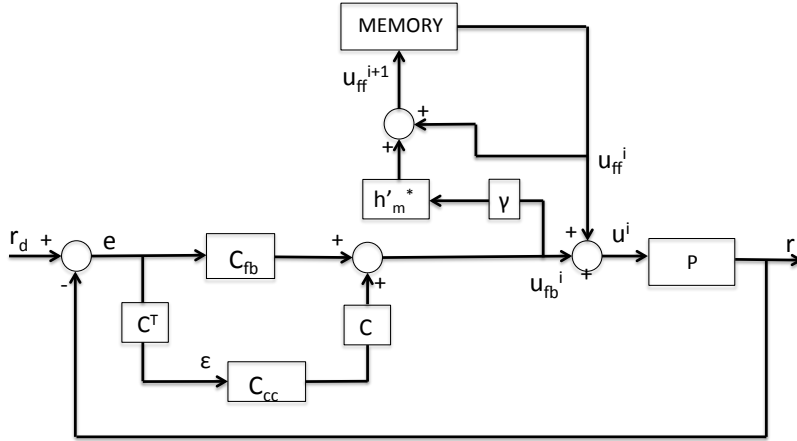
Figure 4.6: Learning Based Cross-coupled Controller for Multi-axis Systems

4.4 Stability and Convergence

Analizing the stability of a control design is important to ensure that the controller can stabilize (or won't destabilize) a given system. Design of the proposed control system can be considered through three steps which are designing feedback controllers for each axis, a cross-coupled controller and iterative learning controllers for each axis while considering the cross-coupled control signals. A generalized block diagram of the presented control for multi-axis systems is given in Figure 4.6. Symbols and their explanations are given in TABLE 4.1
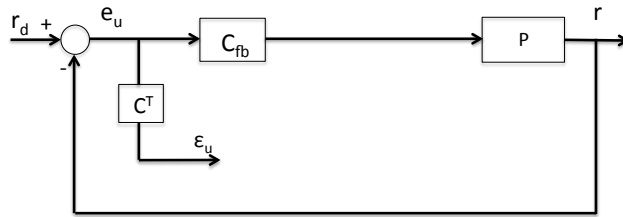
Figure 4.7: Block Diagram of Uncoupled System

Firstly, a stabilizing controller can be designed for each single-axis slider. Then, the designed cross-coupled controller should be stable. For cross-coupled systems, stability can be analyzed through a term called contour error transfer function (CETF). Concept of CETF is introduced by Yeh and Hsu in [41] as

Table 4.1: Parameters

Symbol	Description
$\boldsymbol{r_d} = [r_{dx}, r_{dy}, r_{dz}, ...]^T$	desired input trajectory
$\boldsymbol{r} = [r_x, r_y, r_z, ...]^T$	output trajectory
$\boldsymbol{e} = [e_x, e_y, e_z, ...]^T$	axial tracking error
$\boldsymbol{e} = [e_{ux}, e_{uy}, e_{uz}, ...]^T$	uncoupled axial tracking error
$\boldsymbol{u^i} = [u_x^i, u_y^i, u_x^i, ...]^T$	axial driving signal at i^{th} iteration
$\boldsymbol{u_{fb}^i} = [u_{fbx}^i, u_{fby}^i, u_{fbz}^i, ...]^T$	combined control signal
$\boldsymbol{u_{ff}^i} = [u_{ffx}^i, u_{ffy}^i, u_{ffz}^i, ...]^T$	feedforward control signal at i^{th} iteration
$\boldsymbol{C} = [C_x, C_y, C_z, ...]^T$	coupling gains
$\boldsymbol{C_{fb}} = diag\{C_{fbx}, C_{fby}, C_{fbz}, ...\}$	feedback controller
$\boldsymbol{P} = diag\{P_x, P_y, P_z, ...\}$	axial controlled plant
C_{cc}	cross-coupled controller
γ	learning gain
h'_m*	algebraic averager for ILC
ε	contour error
ε_u	uncoupled contour error

the relationship between a coupled (Figure 4.8) and uncoupled (Figure 4.7) system. Coupled system refers to a system controlled by cross-coupled controller and uncoupled system refers to the same system only without the cross-coupled controller. To derive the CETF, contour error should be derived for systems without and with CCC as ε_u and ε, respectively. Contour error for uncoupled system can be derived as follows

$$\begin{aligned}
\boldsymbol{e_u} &= \boldsymbol{r_d} - \boldsymbol{r} \\
&= \boldsymbol{r_d} - \boldsymbol{P}.\boldsymbol{C_{fb}}.\boldsymbol{e_u} \\
&= (\boldsymbol{I} + \boldsymbol{P}.\boldsymbol{C_{fb}})^{-1}.\boldsymbol{r_d}
\end{aligned} \quad (4.3)$$

$$\begin{aligned}
\varepsilon_u &= \boldsymbol{C}^T.\boldsymbol{e_u} \\
&= \boldsymbol{C}^T.(\boldsymbol{I} + \boldsymbol{P}.\boldsymbol{C_{fb}})^{-1}.\boldsymbol{r_d}
\end{aligned} \quad (4.4)$$
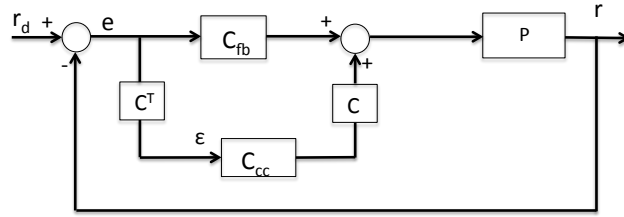
Figure 4.8: Block Diagram of Coupled System

For the coupled system, contour error is calculated as follows:

$$
\begin{aligned}
\boldsymbol{e} &= \boldsymbol{r_d} - \boldsymbol{r} \\
&= \boldsymbol{r_d} - \boldsymbol{P}.(\boldsymbol{C_{fb}}.\boldsymbol{e} + \boldsymbol{C}.C_{cc}.\boldsymbol{C^T}.\boldsymbol{e}) \\
&= (\boldsymbol{I} + \boldsymbol{P}.\boldsymbol{C_{fb}} + \boldsymbol{C}.C_{cc}.\boldsymbol{C^T})^{-1}.\boldsymbol{r_d}
\end{aligned}
\tag{4.5}
$$

$$
\begin{aligned}
\varepsilon &= \boldsymbol{C^T}.\boldsymbol{e} \\
&= \boldsymbol{C^T}.(\boldsymbol{I} + \boldsymbol{P}.\boldsymbol{C_{fb}} + \boldsymbol{C}.C_{cc}.\boldsymbol{C^T})^{-1}.\boldsymbol{r_d}
\end{aligned}
\tag{4.6}
$$

CETF, the relation between uncoupled and coupled system is as given below as H

$$
\varepsilon = H.\varepsilon_u
\tag{4.7}
$$

Combining (4.4), (4.6) and (4.7), then using matrix inversion lemma, CETF is found as

$$
\begin{aligned}
H = 1 &- \boldsymbol{C^T}.(\boldsymbol{I} + \boldsymbol{P}.\boldsymbol{C_{fb}})^{-1} \\
&.[\boldsymbol{P}^{-1} + \boldsymbol{C}.C_{cc}.\boldsymbol{C^T}(\boldsymbol{I} + \boldsymbol{P}.\boldsymbol{C_{fb}})^{-1}]^{-1}
\end{aligned}
\tag{4.8}
$$

After some simplifications, CETF becomes

$$
\begin{aligned}
H &= \frac{1}{1 + \boldsymbol{C^T}.(\boldsymbol{I} + \boldsymbol{P}.\boldsymbol{C_{fb}})^{-1}.\boldsymbol{P}.C_{cc}.\boldsymbol{C}} \\
&= \frac{1}{1 + P_e C_{cc}}
\end{aligned}
\tag{4.9}
$$

where $P_e = \boldsymbol{C^T}(\boldsymbol{I} + \boldsymbol{P}.\boldsymbol{C_{fb}})^{-1}.\boldsymbol{P}.\boldsymbol{C}$ and can be considered as an equivalent controlled plant. In P_e, $\boldsymbol{C}$ is the cross coupling gains vector and the gain values

are changing between -1 and 1 throughout the motion. Therefore, the equivalent controlled plant has varying parameters. Although these gains vary during the motion, they are not iteration varying because they are related to the reference contour. Considering CETF, H, as the sensitivity function, the cross-coupled controller can be designed using conventional single-input-single-output control methods. Therefore, a stabilizing controller C_{cc} can be designed for this system using traditional feedback stability and robustness techniques after each single-axis loop is designed to be stable. Moreover, according to the theorem given in [41], cross-coupled system is internally stable if single-axis feedback controllers achieve internal stability for each axis and the cross-coupled controller keeps the equivalent control system(C_{cc}, P_e) internally stable while the coupling gains vary. Block diagram of the equivalent control system is given in Figure 4.9
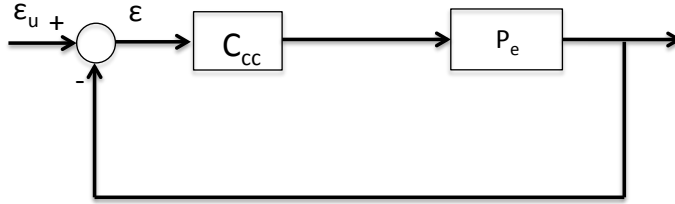
Figure 4.9: Block Diagram of Equivalent Control System

Convergence of the ILC via zero phase filtering on a cross-coupled system can be shown extending the convergence analysis for the single-axis system given in [3]. For the convergence of analysis, some assumptions should be made. Firstly, single-axis plants should be stabilizible and internally stable as well as the cross-coupled control system itself. Furthermore, the number of inputs should be equal to the number outputs in the system. There should be unique desired input u^d for a desired trajectory r_d. Considering control signals as an indication of plant dynamics, system dynamics, u^i can be separated into its repeated and unrepeated components as u_R^d and u_{NR}^i, respectively where the unrepeated part is bounded by $h_m' * u_{NR}^i \leq \varepsilon^*$ for $\forall i$.

$$u^i = u_R^d + u_{NR}^i \tag{4.10}$$

36

According to the theorem given in[3], u_{ff}^i approaches u_R^d as i increases when $\varepsilon^* \to 0$ if the assumptions are satisfied and a task is performed repeatedly. In real aplications, ε^* is very small and can be assumed as $\varepsilon^* \approx 0$. Therefore, while ε^* tends to zero

$$\lim_{i \to \infty} u_{ff}^i = u_R^d \tag{4.11}$$

For the proposed control system, ILC via zero phase filtering is applied to the all single-axis loops. Since all axis trackings are convergent, the contour error is also convergent. Convergence of the RMS (root mean square) contour error is shown in Figure 4.10 for both simulation and experiment. Convergence analysis for simulations and experiments are performed for the trajectories given simulation and experiments chapter. As can be observed from (a) of Figure 4.10, RMS contour error for simulations converges to a value which is very close to zero. For the experiments, convergence is not as smooth as the simulations due to unrepeated disturbances and nonlinearities that are not modeled. RMS contour error converges to a value around $30nm$. Convergence to $30nm$ RMS contour error value can be considered as a good result since encoder resolution used for the experiments is $25nm$.
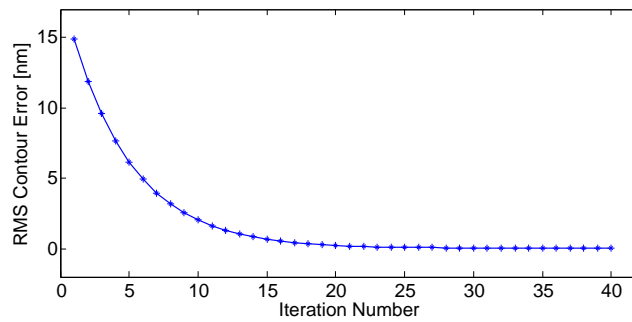
(a)
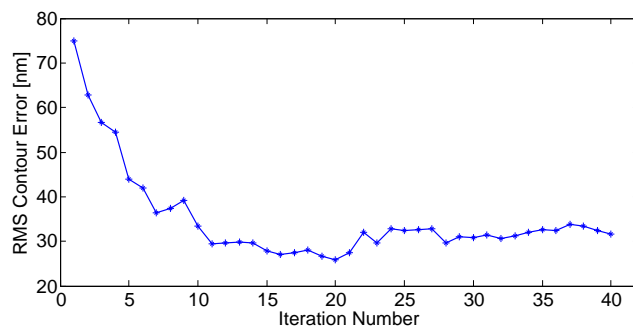
(b)

Figure 4.10: RMS Contour Error for (a) Simulation and (b) Experiment

Chapter 5

Simulation and Experiment

In order to verify the performance of the positioning system, simulation analysis and experiments are conducted for single-axis, two-axis and three-axis positioning systems. For both simulations and experiments, velocity profiling has been used to generate individual-axis reference trajectories. Generic s-curve method is employed for this purpose. In this chapter, trajectory planning used for this thesis is explained. Then, simulation and experimental results of single-axis, two-axis and three-axis system are given respectively.

5.1 Trajectory Planning

With the increased demand from the industry, positioning systems are required to have both high precision and high speed operation capabilities in recent years. However, uncontrolled accelerating or decelerating motion causes residual vibrations during high-speed operation. Hence, the accuracy of the system decreases whereas the settling time increases. However, residual vibrations can be prevented by planning the reference trajectory of the system in a way that acceleration and deceleration phases are smoothed out [42, 43, 44]. This kind of trajectory planning is mostly done by various optimization methods based on the time derivative of the acceleration (i.e., jerk).
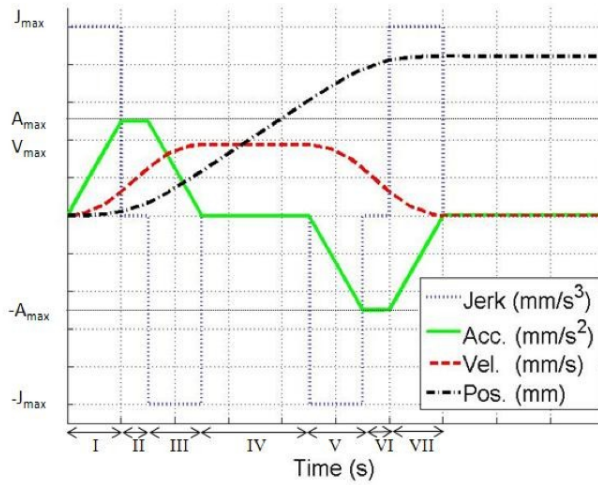
Figure 5.1: A Pulse Shaped Jerk Profile and Its First, Second and Third Integrals as Acceleration, Velocity and Position Profiles

In this section, motion of the stage is planned so that the stage moves smoothly, increasing the accuracy and speed of the motion. Figure 5.1 shows jerk, acceleration, velocity, and position profiles of a typical point to point trajectory, called as s-curve profile. The motion is composed of three regions. These are acceleration region (I to III), constant velocity region (IV), and decelerating region (V to VII). At region II, the maximum acceleration and at region VI, the minimum acceleration is reached and the acceleration is kept constant at these phases of the motion. However, for our system, since the track of the motion is limited by 120mm, it is impossible for the slider to reach the maximum possible acceleration and velocity during its motion between any two points. Hence, regions II, IV, and VI in Figure 5.1 are not present so that the motion is accomplished in maximum and minimum jerk regions only. In the single-axis slider system, magnitudes of maximum and minimum jerk are the same and they can be chosen between 0 to $5000mm/s^3$. Moreover, durations for maximum and minimum jerk regions (I, III, V, and VII) are calculated automatically depending on the specified jerk magnitude and the desired position value.

The same trajectories are used in both experiments and simulations for each

positioning system configurations. However, different trajectories should be generated for each different contour with different dimensions. Constructed trajectories for single-axis slider, two-axis and three-axis system are given in Appendix C.

5.2 Single-axis Slider System

For the single-axis slider system, performance of the system with only feedback control and feedback control with iterative learning control is compared. A generic s-curve trajectory is given to the single-axis system.

5.2.1 Simulation Results

Position results and position error results are given in Figure 5.2 and Figure 5.3, respectively. For the single-axis system simulations, very good tracking performance can be achieved for feedback control with RMS tracking error of $0.76nm$. When iterative learning control is used for 20 executions, system performans becomes even better with $0.05nm$ RMS tracking error. From these simulation results, it can be said that iterative learning control implementation is effective.
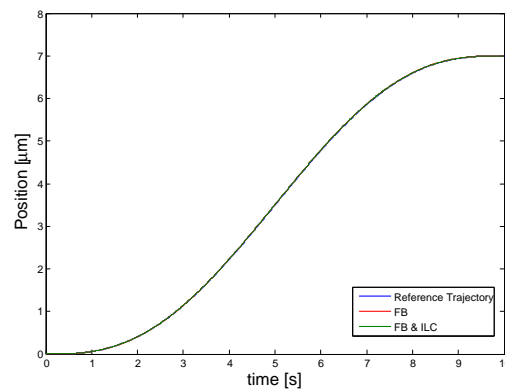
Figure 5.2: Single-axis System Simulation - Position Tracking
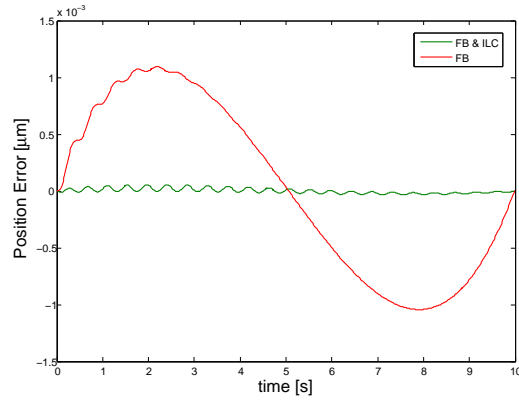
Figure 5.3: Single-axis System Simulation- Position Error

5.2.2 Experimental Results
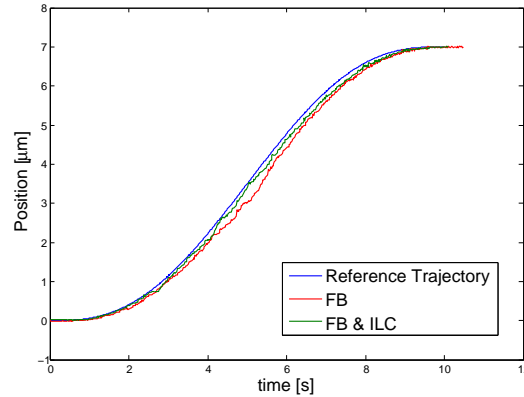
Figure 5.4: Single-axis System Experiment - Position Tracking

Performance of the system with only feedback control and feedback control with iterative learning control is compared by conducting experiments on the single-axis slider system. In this section, results of the experiment conducted on vertical positioning system are provided. Position with respect to time plot is given in Figure 5.4. From the figure, tracking performance improvement of iterative learning control can be observed. In Figure 5.5, tracking error of the single-axis system is given. After 20 iterations, tracking error reduces significantly. In addition to the general reduction, maximum tracking error is decreased from $350nm$ to $100nm$. Moreover, RMS tracking error of $115.29nm$ can be achieved

by feedback control. When iterative learning control is used for 20 executions, system performans enhanced and the RMS tracking error becomes $29.3nm$.
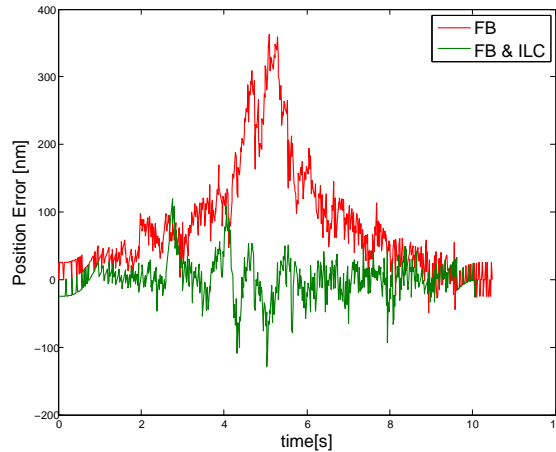
Figure 5.5: Single-axis System Experiment- Position Error

5.3 Two-axis Slider System

In order to verify the performance of the learning based cross-coupled control algorithm, simulations and experiments are conducted on the two-axis positioning system. In the simulations and experiments, performance of the learning based cross-coupled controller is compared with feedback control, feedback control with iterative learning control, feedback control with cross-coupled control. Learning based controller is mentioned as feedback control with cross-coupled control and iterative learning control (FB CCC ILC).

5.3.1 Simulation Results

Two-axis positioning system has been simulated with a nonlinear contour. In the proposed approach, it is straightforward to find coupling gains when the equation of the curve is known since coupling gains are just elements normal vector elements of the contour. This is accomplished through the coupling gain MATLAB script mentioned in related section. Plant model is simulated with

43

feedback control (FB), feedback control with cross-coupled control (FB CCC), feedback control with iterative learning control (FB ILC) and feedback control with cross-coupled control and iterative learning control (FB CCC ILC). Effects of all simulated control schemes on the performance are summarized in TABLE 5.1 and Figure5.6. In the table and figure, root mean square (RMS) of the error signals has been used. It can be observed that combining ILC and CCC with FB gives the best results as expected. This combination benefits from both tracking performance improvements of ILC and contouring performance improvements of CCC. For the designed control system, ILC convergence has been achieved around 20 iterations. In other words, there is no significant decrease in the errors after 20 iterations. Hence, FB ILC and FB CCC ILC simulation results are recorded after 20 iterations.

Table 5.1: Two-axis System simulation - RMS error values for the nonlinear contour

RMS Error in	x-axis[nm]	y-axis[nm]	contour[nm]
FB	11.30	111.27	39.04
FB CCC	15.42	110.65	32.36
FB ILC	3.47	2.17	2.73
FB CCC ILC	1.09	2.11	0.78
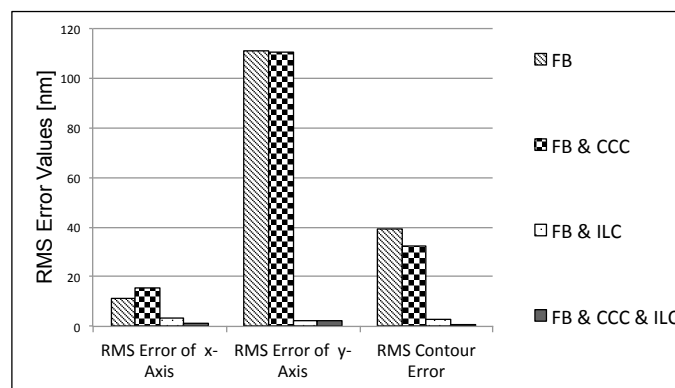
Figure 5.6: Two-axis System Simulation - RMS Error Values for The Nonlinear Contour

The nonlinear contour used in simulations is given in Figure 5.7. In the figure, the zoomed view is taken from the part with a sharp turn that is shown with the box on the original contour because contour tracking is more difficult on sharp
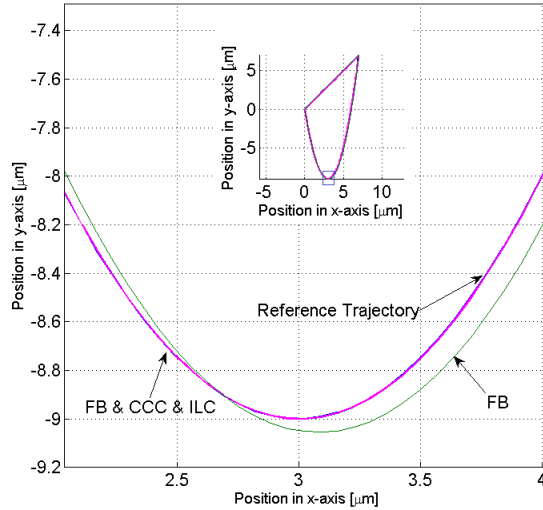
Figure 5.7: Two-axis System Simulation for The Nonlinear Contour

turns. As can be seen in zoomed view of Figure 5.7, contouring performance of the system for the nonlinear contour is improved significantly when the proposed method (FB CCC ILC) is used instead of only feedback (FB) control.

5.3.2 Experimental Results

Velocity profiling with s-curve is used to obtain individual axis trajectories in the experimental results section. For experimental results, the same contour with same velocity profiling designed for simulations part is used. Contour tracking of the two-axis system with only feedback (FB) control and feedback control with CCC and ILC (FB CCC ILC) is given in Figure 5.8. Looking at the zoomed view, it is obvious that presented control design improved contouring performance considerably. When (a) and (b) of Figure 5.8 is compared, it should be noted that simulations and experiments give similar behavior such as deteriorated contour control just after the sharp turn. Moreover, FB CCC ILC system gives better contouring result than FB. Yet, in experimental results, FB CCC ILC design does not improve the contouring performance as much as simulation. This result is reasonable considering unmodeled system dynamics or disturbances.
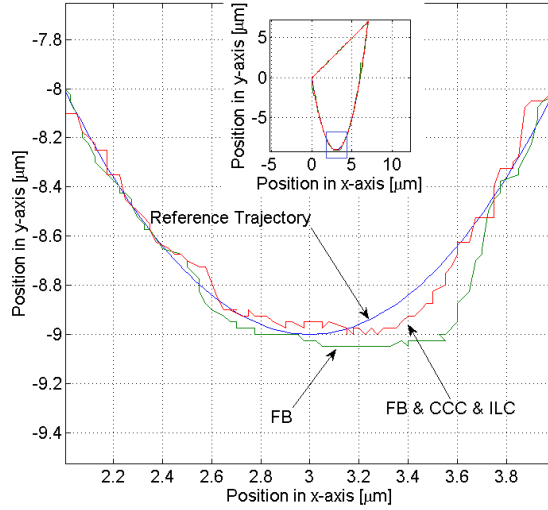
Figure 5.8: Experimental Results of Two-axis System for The Nonlinear Contour

Experiments are conducted on the system with feedback control (FB), feedback control with cross-coupled control (FB CCC), feedback control with iterative learning control (FB ILC) and feedback control with cross-coupled control and iterative learning control (FB CCC ILC). FB ILC and FB CCC ILC experimental results are recorded after 20 iterations. Variation of RMS single-axis errors and RMS contour error with the different control schemes is given in Figure5.9 and TABLE 5.2. Looking at TABLE 5.2, it can be observed that FB CCC system decreases contour error significantly whereas changes in axial errors are not as significant. Similarly, FB ILC system decreases axial tracking errors more effectively than contour error as expected. Best tracking and contouring performance is obtained for FB CCC ILC system as for the simulation case. All axial tracking errors and contour error are improved around 50%. This improvement is higher for simulations however this is acceptable since simulations are performed for idealized systems in idealized conditions.

Table 5.2: Two-axis System experiments - RMS error values for the nonlinear contour

RMS Error in	x-axis[nm]	y-axis[nm]	contour[nm]
FB	46.84	113.05	57.08
FB CCC	42.06	94.66	43.49
FB ILC	25.81	79.14	39.33
FB CCC ILC	21.28	66.69	27.52
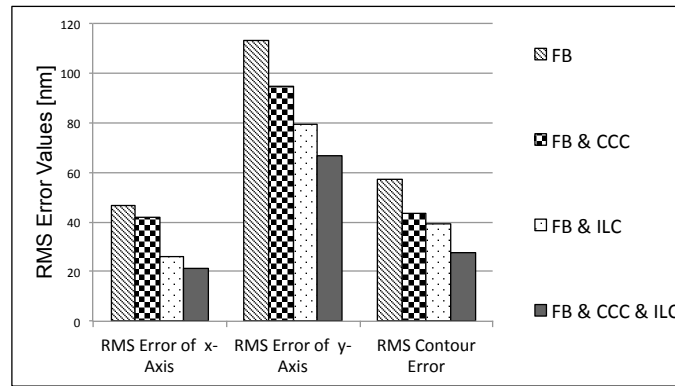
Figure 5.9: Two-axis System Experiment - RMS Error Values for The Nonlinear Contour

5.4   Three-axis Slider System

Performance of the learning based cross-coupled controller is also tested on three-axis system. In this work, it is also claimed that the proposed method can be implemented on a three-axis system. In order to demonstrate it, simulations and experiments of proposed method for three-axis system are supplied. In the simulations and experiments, performance of the learning based cross-coupled controller is compared with feedback control, feedback control with iterative learning control, feedback control with cross-coupled control. Learning based controller is mentioned as feedback control with cross-coupled control and iterative learning control (FB CCC ILC). Reference contour is a 45 *degrees* inclined circle with 7 *micrometers* radius as given in Figure 5.10 . As mentioned previously, coupling gains can be obtained from the normal vector of the contour. Using that approach coupling gains have been found without too much computational effort.

5.4.1 Simulation Results

In the zoomed view of Figure 5.10, it has been observed that the proposed method has very good tracking performance compared with the feedback control. Moreover, reference contour and the resulting contour of the FB CCC ILC control is almost coincident. This also confirms the very small RMS tracking errors and RMS contour error observed in TABLE 5.3.

Simulation results of three-axis system given in TABLE 5.3 and Figure 5.11. Looking at the results, it is observed that contour error decreases with FB CCC whereas individual axis errors may deteriorate. Yet, when the ILC is also added to the control scheme both individual and contour errors decrease significantly. For these simulations, combined CCC and ILC gives the best contour and tracking accuracy. Moreover, it can also be observed that FB ILC control decreases individual axis tracking errors by 63%, 85%, 63%, contour error 46%. When CCC is added to FB ILC controls contour error decreases 72% and individual tracking errors decrease by 36%, 43% and 63%. This observation confirms ILC is especially efficient in tracking control whereas CCC is especially effective for contour control. Moreover, combining both controllers results in a controller, which is effective for both tracking and contouring.
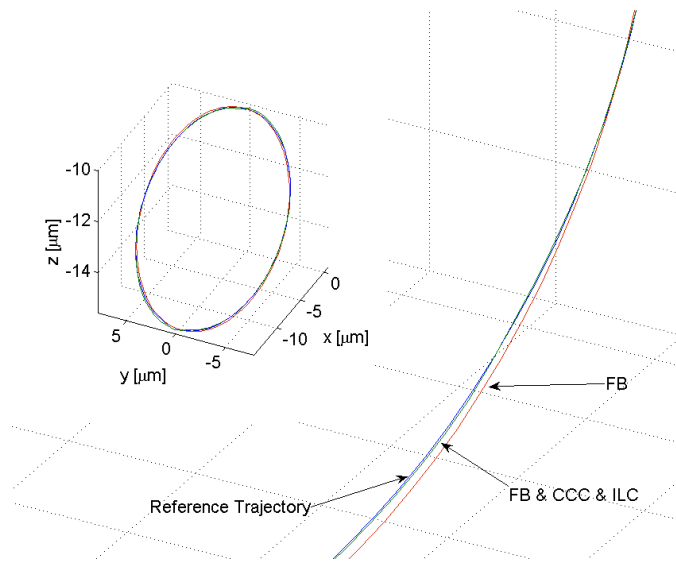
Figure 5.10: Three-axis System Simulation for The Nonlinear Contour

48

Table 5.3: Three-axis system simulation - RMS error values for the nonlinear contour

RMS Error in	x-axis[nm]	y-axis[nm]	z-axis[nm]	contour[nm]
FB	235.87	144.26	235.87	86.07
FB CCC	268.06	177.19	209.68	59.12
FB ILC	33.07	51.44	33.07	46.29
FB CCC ILC	21.22	29.78	12.29	13.55
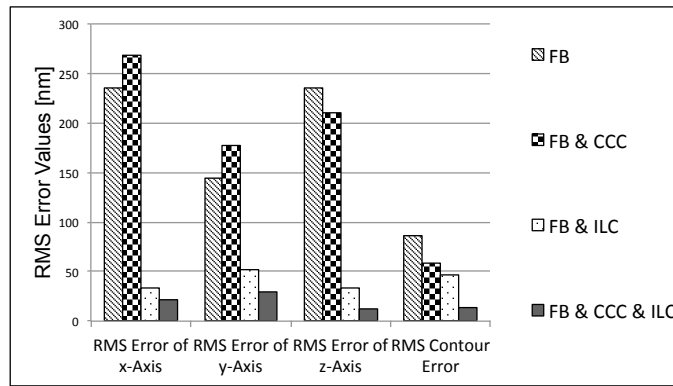
Figure 5.11: Three-axis System Simulation - RMS Error Values for The Nonlinear Contour

5.4.2 Experimental Results

Three-axis system experiments are conducted on the system with feedback control (FB), feedback control with cross-coupled control (FB CCC), feedback control with iterative learning control (FB ILC) and feedback control with cross-coupled control and iterative learning control (FB CCC ILC) which is the learning based cross-coupled controller. FB ILC and FB CCC ILC experimental results are recorded after 20 iterations since after 20 iterations improvements are not obvious as before. Variation of RMS single-axis errors and RMS contour error with the different control schemes is given in Figure 5.12 and TABLE 5.4. Looking at TABLE 5.4, it can be observed that FB CCC system decreases contour error significantly whereas axial error for z-axis increases a little bit. This is acceptable since cross-couples control promises to improve contour error while axial tracking may deteriorate. Also, contouring performance is the important criteria for multi-axis systems rather than axial-tracking errors. Similarly, FB ILC system

decreases axial tracking errors more effectively than contour error as expected. Best tracking and contouring performance is obtained for FB CCC ILC system as for the simulation case. Moreover, having maximum RMS error as $76.86nm$ is fairly good for a system with $25nm$ encoder resolution. Although simulations show better improvement on tracking and contouring, this is expected since simulations are performed for idealized conditions.

Table 5.4: Three-axis system experiment - RMS error values for the nonlinear contour

RMS Error in	x-axis[nm]	y-axis[nm]	z-axis[nm]	contour[nm]
FB	135.16	99.97	213.43	137.95
FB CCC	70.71	86.56	229.72	74.04
FB ILC	72.56	81.60	34.90	57.45
FB CCC ILC	53.55	76.86	34.41	43.61
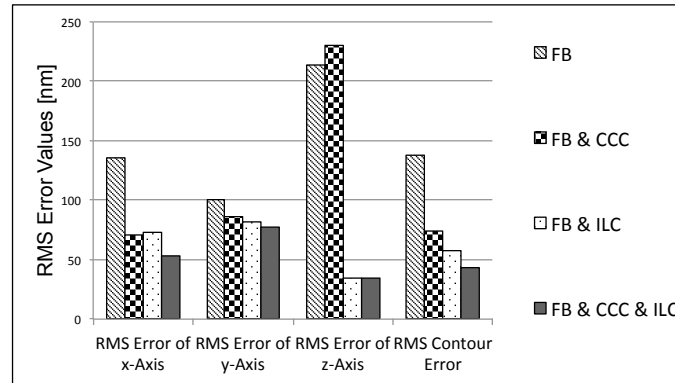
Figure 5.12: Three-axis System Experiments - RMS Error Values for The Nonlinear Contour

In Figure 5.13, contour tracking of the system is given for x-y plane projection, y-z plane projection, x-z plane projection and x-y-z three dimensional view. Looking at these figures, benefits of the proposed controller for contour tracking is obvious.
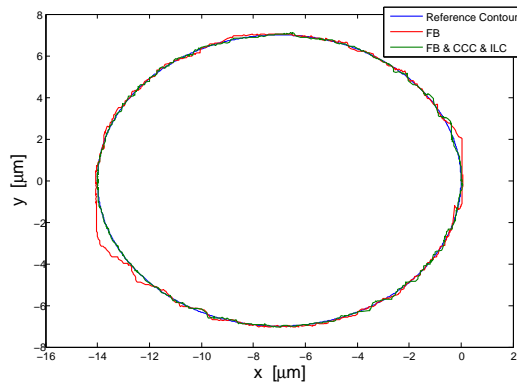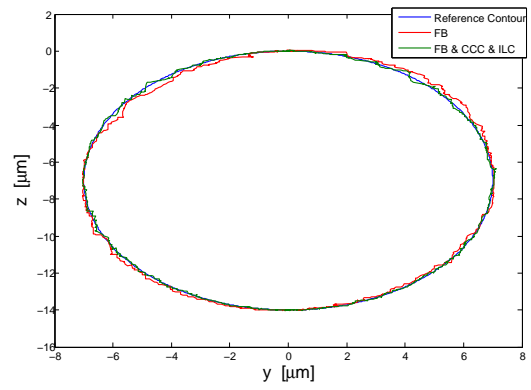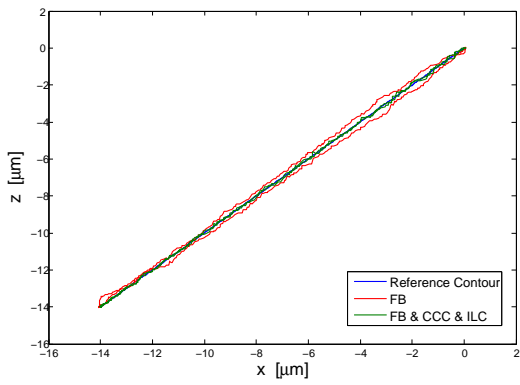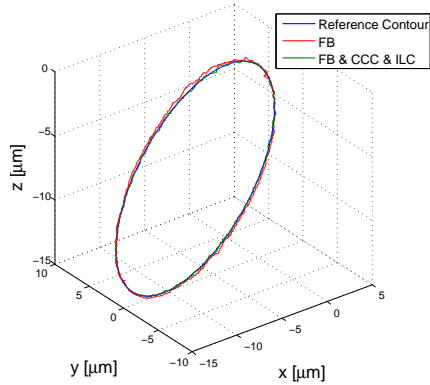
Figure 5.13: (a) x-y Plane, (b) y-z Plane, (c) x-z Plane and (d) 3 Dimensional Experimental Results of Three-axis System for The Nonlinear Contour

Chapter 6

Robustness

It is important for a system to stay stable under reasonable variations in system parameters and disturbances. In addition to staying stable, performance of the system should be in an acceptable margin in the existence of uncertainties and disturbances. In this chapter, robustness of the control design is tested through some experiments. First, predicted uncertainties and disturbances of the system are described. Then, the test setup that is used to simulate these uncertainties and disturbances for the experiments is explained. Finally, test results are provided with the conclusions withdrawn.

6.1 Predicted Uncertainties and Disturbances of the System

In order to test the robustness of the system, first, test parameters should be determined. For the determination of test parameters, there are two important concerns as the controlled system and the application that it is used for. The system should be examined carefully to indicate the uncertainties and nonlinearities. Moreover, the application is very important in terms of the disturbances. Variations of the system parameters may also depend on the application.

For our slider system, mathematical model is derived with idealizations in permanent magnet linear motor and bearings. In permanent magnet linear motors, there are force ripples that depend on position. These ripples are generally small in magnitude and position dependent [45]. Since the force ripples are small fluctuations on the motor force, an axial force in the direction of movement of the slider can represent this uncertainty (Figure 2.6). For idealization of cross-roller bearings, friction force is modeled as only viscous friction. However, there are other friction models that should be considered as coulomb and stribek friction. Since there are unmodeled and nonlinear effects in friction, these should be represented in the test. Similarly, friction forces can be symbolized by a force in the movement axis.

Application that the positioning system is used for is very important when disturbances applied on it are considered. For example, a part will be assembled on the system for any application in order to be positioned. This part could be a laser head with small mass or it could be a larger part to be machined. Therefore, the control design should withstand the mass of assembled parts up to a certain value. During the tests, this can easily be represented by adding mass on the two-axis positioning system. Yet, three-axis positioning system includes a vertical axes and counter balance. Additional mass assemblies are compansated by the adjustable air counter balance system in our system. Depending on the application, axial disturbances can also change. For example, surface scanning creates only small disturbances at the point of touch. Yet, average cutting force is about $2-3N$ for micro-machining applications [46]. These disturbances can be represented as axial forces in the robustness tests. Moreover, there can be sudden changes in the cutting force due to impurities in the in the material. Applying sudden axial forces could be a representation of this disturbance in the robustness tests.

6.2   Test Setup

In the previous section, predicted uncertainties and disturbances are explained. Some ways to represent these uncertainties and disturbances in the experiments are also discussed. All uncertainties and disturbances of the system can be symbolized by three methods as assembling additional sliding mass, applying constant axial force and applying sudden axial force. In order to perform these tests, the test setup given in Figure 6.1 is used. In this setup, pulley systems are used to obtain axial forces by hanging parts with specific mass. Additional mass tests are performed by assembling the parts with specific mass on the positioning system. For three-axis positioning system, there is also a vertical axis in addition to the horizontal axes. For a vertical axes axial forces can be represented by assembling mass on the slider but without adjusting the counter balance system for the current sliding mass. Axial forces are applied through assembling mass on the vertical axis and using the pulley system for horizontal axes.
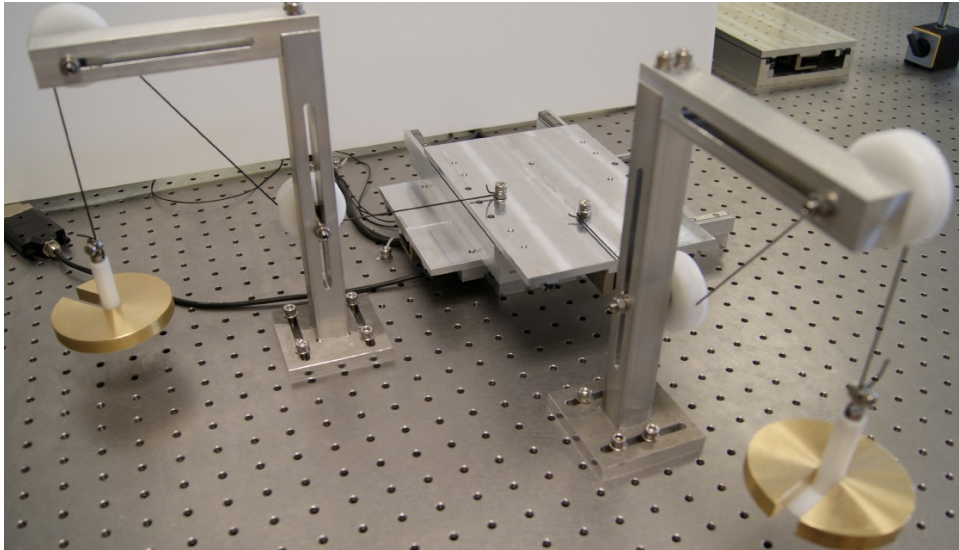

Figure 6.1: Robustness Test Setup

6.3 Test Results

As explained, three different types of experiments should be carried out. These three test types are sliding mass increase test, constant axial force test and sudden axial force test. Next three subsections will discuss result of these test. Experimental results of the system without artificial uncertainties and disturbances are given in Section 5.3.2 for $25nm$ encoder resolution. Also, the same contour and trajectories are used for robustness tests. As mentioned before, sensitivity of the system to electrical noises increases for lower encoder resolution values. In order to distinguish effects of the physical noises from electrical noises, $33nm$ encoder resolution is used since system is less sensitive to electrical noises at this resolution level. Moreover, experiments are conducted at the end of the sliders since limits of the linear motor show least effecient performance. Therefore, experiments are performed for worst phsycal conditions.

6.3.1 Sliding Mass Increase Test

Table 6.1: Sliding Mass Inrease Test Results for 1st Run

Additional Mass	250g	500g	1000g
RMS x-axis error [nm]	45	43	119
RMS y-axis error [nm]	140	200	81
RMS contour error [nm]	63	110	78

Table 6.2: Sliding Mass Inrease Test Results for 20th Run

Additional Mass	250g	500g	1000g
RMS x-axis error [nm]	31	33	41
RMS y-axis error [nm]	100	92	101
RMS contour error [nm]	51	51	60

For sliding mass increase tests, $250g$, $500g$ and $1000g$ masses are assembled on the positioning system. As mentioned in the previous section, sliding mass increase can be compansated through counter balance system for the vertical axis.

55

Therefore, sliding mass increase tests are performed for only two-axis positioning system. Test results for the 1st run are summarized in Table 6.1. As expected, system performance is deteriorated when extra mass is assembled compared to the results given in Section 5.3.2. Since the disturbances in these test are repeatable, learning based cross-coupled controller helps system to compansate for the increase in mass. After 20 iterations, system shows similar performances for all extra mass values and error values are decreased as can be observed from Table 6.2. Results of the 20th run are fairly good considering encoder resolution is $33nm$. When these results are compared with the ones without any artificial uncertainty and disturbance, it can be concluded that system performance is acceptable for sliding mass increase up to $1000g$.

6.3.2 Constant Axial Forces Test

Table 6.3: Constant Axial Force Test in x-axis for 1st Run (two-axis system)

Magnitude of Force	1N	2.5N	5N
RMS x-axis error [nm]	78	150	170
RMS y-axis error [nm]	340	340	330
RMS contour error [nm]	200	210	230

Table 6.4: Constant Axial Force Test in x-axis for 20th Run (two-axis system)

Magnitude of Force	1N	2.5N	5N
RMS x-axis error [nm]	32	57	39
RMS y-axis error [nm]	120	88	85
RMS contour error [nm]	68	59	55

Table 6.5: Constant Axial Force Test in y-axis for 1st Run (two-axis system)

Magnitude of Force	1N	2.5N	5N
RMS x-axis error [nm]	85	65	76
RMS y-axis error [nm]	750	1000	1200
RMS contour error [nm]	300	370	450

Table 6.6: Constant Axial Force Test in y-axis for 20th Run (two-axis system)

Magnitude of Force	1N	2.5N	5N
RMS x-axis error [nm]	28	43	27
RMS y-axis error [nm]	190	170	200
RMS contour error [nm]	64	82	64

Table 6.7: Constant Axial Force Test in both x and y axes for 1st Run (two-axis system)

Magnitude of Force	1N	2.5N	5N
RMS x-axis error [nm]	110	140	160
RMS y-axis error [nm]	850	1000	1300
RMS contour error [nm]	320	390	490

For the experiments of this subsection, constant axial forces with magnitude of $1N$, $2.5N$ and $5N$ are applied on the system using the test setup given in Figure 6.1. Robustness of the control system to constant axial forces is tested through three sets of experiments as constant axial force in only x-axis, only y-axis and both x-axis and y-axis on the two-axis system. Moreover, for three-axis sytem, constant axial force tests are conducted in only z-axis and all axes (x-y-z) together.Test results of constant axial force in only x-axis, only y-axis and both x-axis and y-axis are summarized in Table 6.3, Table 6.5 and Table 6.7, respectively for $1^{st}run$. After 20 iterations, system gives improved contour error values for all constant axial force tests as can be observed from Table 6.4, Table 6.6 and Table 6.8. Three axis system test results are summerized in Table 6.9 and Table 6.11 for $1^{st}run$ of only z-axis and x-y-z axes tests, respectively. The $20^{th}run$ results of these tests are given in Table 6.10 and Table 6.12. It is observed that learning based cross-coupled controller is efficient to reduce effects of these repeated disturbances. Overall performance of the control system is in the acceptable range in the existence of constant axial forces.

Table 6.8: Constant Axial Force Test in both x and y axes for 20th Run (two-axis system)

| Magnitude of Force	1N	2.5N	5N
RMS x-axis error [nm]	47	30	29
RMS y-axis error [nm]	190	160	190
RMS contour error [nm]	66	66	69
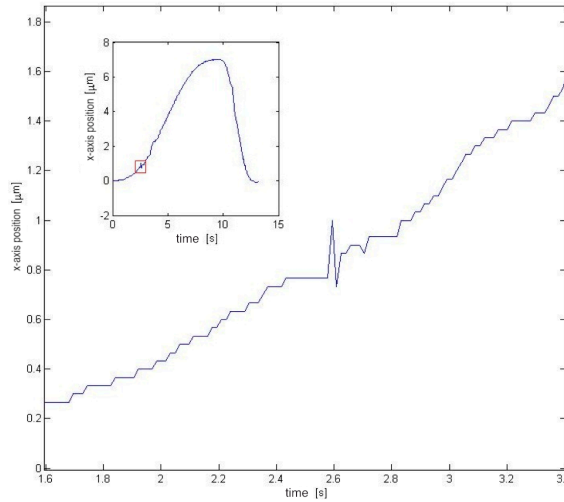
Figure 6.2: System Response with 0.1N Sudden Axial Force for Horizontal Axis

6.3.3   Sudden Axial Force Test

Lastly, this section discusses the robustness of the control system in the existence of sudden axial forces. For our system, sudden axial force may be caused by a sudden electrical noise or an impurity in the machined part during a machining operation etc. These sudden changes assumed to be small in magnitude. In the experiments, axial forces of $0.02N$, $0.05N$ and $0.1N$ are applied suddenly. Effects of these small sudden forces can not be observed through root mean square of errors. Graphical representations are better to show effects of sudden disturbances. For forces of $0.02N$ and $0.05N$, effects are very small that they can not be observed by encoder measurement resolution of $33nm$. In Figure 6.2, trajectory response of x-axis is given for sudden axial force of $0.1N$ with its
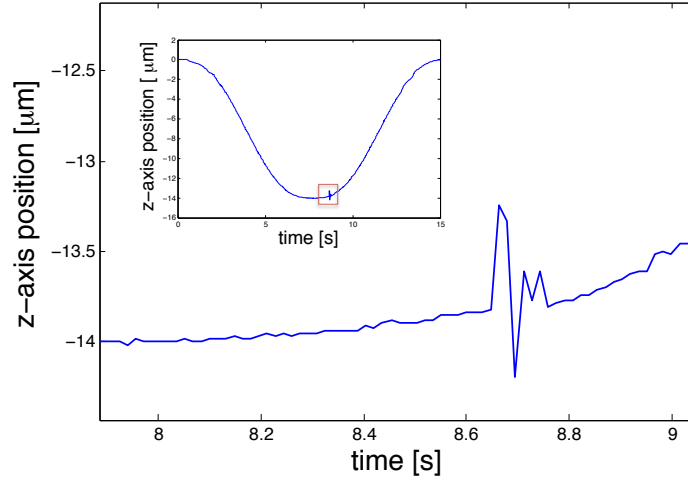
Figure 6.3: System Response with 0.1N Sudden Axial Force for Vertical Axis

Table 6.9: Constant Axial Force Test in z axis for 1st Run (three-axis system)

Magnitude of Force	1N	2.5N	5N
RMS x-axis error [nm]	164	116	176
RMS y-axis error [nm]	134	169	141
RMS z-axis error [nm]	222	223	221
RMS contour error [nm]	89	99	104

zoomed view to represent the response of a horizontal slider. Trajectory response of z-axis is given in Figure 6.3 to represent vertical slider response. Looking at the figures, it can be said that system can absorb this disturbance in acceptable time duration with an acceptable deflection.

6.4   Conclusion

In this section, series of experiments have been conducted to examine robustness of the learning based cross-coupled control system. Since learning based cross-coupled controller utilizes iterative learning control, repeated disturbances are compensated through iterations. For a multi-axis system, contour error is the most important criteria. In the robustness test results, RMS contour error

Table 6.10: Constant Axial Force Test in z axis for 20th Run (three-axis system)

Magnitude of Force	1N	2.5N	5N
RMS x-axis error [nm]	93	105	193
RMS y-axis error [nm]	116	102	108
RMS z-axis error [nm]	35	45	59
RMS contour error [nm]	52	64	73

Table 6.11: Constant Axial Force Test in all x-y-z axes for 1st Run (three-axis system)

Magnitude of Force	1N	2.5N	5N
RMS x-axis error [nm]	120	152	164
RMS y-axis error [nm]	249	449	537
RMS z-axis error [nm]	217	226	204
RMS contour error [nm]	80	158	143

is always below $82nm$ after 20 iterations. For $33nm$ encoder resolution and the existing disturbances, maximum of $82nm$ RMS contour error is fairly good. Although system shows satisfactory results for the sudden disturbances, proposed controller is not designed for systems with large sudden disturbances since sudden disturbances generally unrepeated disturbances. If the positioning system is used for an application involving large sudden disturbances, a robust controller can be designed. The proposed controller uses PID controller as a feedback control scheme, replacing it with a robust control scheme could result in better performance in the existence of disturbances. In other words, a robust feedback controller, feed-forward iterative learning controller and cross-coupled controller can be used together to obtain an integrated controller with increased robustness.

Table 6.12: Constant Axial Force Test in all x-y-z axes for 20th Run (three-axis system)

Magnitude of Force	1N	2.5N	5N
RMS x-axis error [nm]	37	40	37
RMS y-axis error [nm]	68	93	90
RMS z-axis error [nm]	33	35	34
RMS contour error [nm]	46	46	38

Chapter 7

Conclusion and Future Work

In this thesis, a MIMO controller featuring cross-coupled control and iterative learning control schemes is presented to improve contour and tracking accuracy at the same time. Instead of using the standard contour estimation technique proposed with the variable gain cross-coupled control, presented control design incorporates a computationally efficient contour estimation technique. In addition to that, implemented contour estimation technique makes the presented control scheme more suitable for arbitrary nonlinear contours and multi-axis systems. The presented control system is intended to be modular considering that the stages can be interchanged without changing the control system. For modularity concerns, ILC is chosen to improve tracking performance since controller structure does not change with plant model structure and parameters changes. Also, using the zero-phase filtering based iterative learning control results in a practical design and an increased applicability to modular systems. It is observed that the same control parameters for ILC via zero-phase filtering resulted in sufficient convergence for all configurations of the single-axis system (x, y and z). Furthermore, use of ILC is beneficial for modular systems to compensate the changes after the assembly due to its learning nature.

Stability and convergence analysis of the learning based cross-coupled controller is also provided. Tracking and contouring performance of the method

on a nonlinear contour is verified through simulations and experiments achieving nanometer level accuracy for the two-axis and three-axis positioning systems. Simulation and experimental testing of the different controllers demonstrated contouring performance benefits from the combined feedback (FB), iterative learning (ILC) and cross-coupled control (CCC) system. Four different control methods as FB, FB I LC, FB CCC, FB CCC ILC were tested. The best control system was found to be the combination of FB, ILC and CCC, which resulted in both the best individual axis and contour tracking performances.

Tracking and contouring performance of the method on a nonlinear contour is verified through simulations and experiments achieving nanometer level accuracy for the two-axis system. In the experiments, RMS error of x-axis, RMS error of y-axis and RMS contour error of the two-axis system is decreased to $21nm$, $66nm$ and $27nm$, respectively. Considering encoder resolution, the smallest value encoder can detect, is $25nm$, resultant positioning is very accurate. Having RMS error less than the resolution means that trajectory is followed very closely and error value has been zero in some parts of the motion as for case of RMS error of x-axis. For three-axis positioning system experiments, RMS error of x-axis, RMS error of y-axis, RMS error of z-axis and RMS contour error is decreased to $54nm$, $77nm$, $34nm$ and $44nm$, respectively. This result is also very good for a three-axis positioning system operating with $25nm$ encoder resolution.

Robustness of the control algorithm implementation is tested through some experiments that are designed considering the expected disturbances and system uncertainties. These disturbances and uncertainties are modeled regarding some specific applications. In future, the controller performance will be examined using the positioning system for these specific applications such as micro-machining.

Since learning based cross-coupled controller utilizes iterative learning control, repeated disturbances are compensated through iterations. In the robustness test results, RMS contour error is always below $82nm$ after 20 iterations. For $33nm$ encoder resolution and the existing disturbances, maximum of $82nm$ RMS contour error is fairly good. Although system shows satisfactory results for the sudden disturbances, proposed controller is not designed for systems with large

sudden disturbances. If the positioning system is used for an application involving large sudden disturbances, a robust controller can be designed. The proposed controller uses PID controller as a feedback control scheme, replacing it with a robust control scheme could result in more robust performance. In other words, a robust feedback controller, feed-forward iterative learning controller and cross-coupled controller can be used together to obtain an integrated controller with increased robustness.

Bibliography

[1] S. S. Yeh and P. L. Hsu, "Estimation of contouring error vector for the cross-coupled control design," *IEEE/ASME Transaction on Mechatronics*, vol. 7, no. 1, pp. 44–51, 2002.

[2] A. E. Khalick and N. Uchiyama, "Discrete-time model predictive contouring control for design based on iterative contour error estimation for biaxial feed drive systems and experimental verification," *Journal of Mechatronics*, vol. 21, pp. 918–926, 2011.

[3] K. K. Tan, H. Dou, Y. Chen, and T. H. Lee, "High precision linear motor control via zero-phase filtering," *IEEE Transactions on Control Systems Technology*, vol. 9, no. 2, pp. 244–253, 2001.

[4] E. Manske, T. Hausotte, R. Mastylo, T. Machleidt, K. Franke, and G. Jager, "New applications of the nanopositioning and nanomeasuring machine by using advanced tactile and non-tactile probes," *Measurement Science and Technology*, vol. 18, no. 2, pp. 520–527, 2007.

[5] L. Lihua, L. Yingehun, G. Yongfeng, and S. Akira, "Design and testing of nanometer positioning system," *Journal of Dynamic Systems, Measurement and Control*, vol. 132, no. 2, pp. 021011–6, 2010.

[6] C. K. Pang, G. Guo, B. M. Chen, and T. H. Lee, "Self-sensing actuation for nanopositioning and active-mode damping in dual stage HDDs," *IEEE/ASME Transactions on Mechatronics*, vol. 11, no. 3, pp. 328–338, 2006.

[7] N. Gecer-Ulu, E. Ulu, S. Filiz, and M. Cakmakci, "Development of a modular single-axis slider system for high precision positioning applications," in *The 15th International Conference on Machine Design and Production*, 2012.

[8] E. Ulu, N. Gecer-Ulu, and M. Cakmakci, "Adaptive correction and look-up table based interpolation of quadrature encoder signals," in *Proc. ASME Dynamic Systems and Control Conf. (DSCC 2012)*, (Ft. Lauderdale, FL), Oct 2012. To appear.

[9] K. Ogata, *Modern Control Engineering*. Prentice Hall, 1990.

[10] S. Devasia, E. Eleftheriou, and S. O. R. Moheimani, "A survey of control issues in nanopositioning," *IEEE Transactions on Control Systems Technology*, vol. 15, no. 5, pp. 802–823, 2007.

[11] G. J. Maeda, K. Sato, H. Hashaizume, and T. Shinshi, "Control of xy nanopositioning table for a compact nanomachine tool," *JSME Int. J. Ser. C.*, vol. 49, no. 1, pp. 21–27, 2006.

[12] K. J. Astrom and B. Wittenmark, *Adaptive Control:Second Edition*. Dover Publications, 2008.

[13] P. Iannou and B. Fidan, *Adaptive Control Tutorial*. SIAM, Society for Industrial and Applied Mathematics, 2006.

[14] L. Wang, S. Lin, and H. Zeng, "Precision contour control of XY table based on LuGre model friction compensation," in *2nd International Conference on Intelligent Control and Information Processing (ICICIP), IEEE*, pp. 1124–1128, 2011.

[15] Y. Altintas and B. Sencer, "High speed contouring control strategy for five-axis machine tools," *CIRP Annals - Manufacturing Technology*, vol. 59, pp. 417–420, 2010.

[16] M. Tomizuka, "Zero phase error tracking algorithm for digital control," *Journal of Dynamic Systems, Measurement and Control*, vol. 109, no. 1, pp. 65–68, 1987.

[17] P. Hsu, Y. Houng, and S. Yeh, "Design of an optimal unknown unknown input observer for load compensation in motion systems," *Asian Journal of Control*, vol. 3, no. 3, pp. 204–215, 2001.

[18] L. Qing, W. Tai-yong, D. Ying-chuan, J. Yong-xiang, and L. Bo, "Applications of position controller for cnc machines based on state observer and cross-coupled controller," in *International Conference on Computer Mechatronics, Control and Electronic Engineering(CMCE), IEEE*, pp. 593–596, 2010.

[19] M. Tomizuka, "Friction compensator for feed drive systems consisting of ball screw and linear ball guide," in *Proc. of the 35th International MATADOR Conference*, pp. 311–314, 2007.

[20] B. C. Chen, D. M. Tilbury, and A. G. Ulsoy, "Modular control for machine tools: Cross-coupling control with friction compensation," in *Proc. ASME IMECE*, (Anaheim, CA), 1998.

[21] K. L. Barton and A. G. Alleyne, "A cross-coupled iterative learning control design for precision motion control," *IEEE Transactions on Control System Technology*, vol. 16, no. 6, pp. 1218–1231, 2008.

[22] Z. Novakovic, *The Principle of Self Support in Control Systems*, vol. 8. Amsterdam, Netherlands: Elsevier, 1992.

[23] H. S. Ahn, Y. Q. Chen, and K. L. Moore, "Iterative learning control: Brief summary and categorization," *IEEE Transactions on Systems, Man, and Cybernetics, Part C: Applications and Reviews*, vol. 37, no. 6, pp. 1099–1121, 2007.

[24] P. Scholten, "Iterative learning control: Analysis. a design for a linear motor motion system," Master's thesis, University of Twente, 2000.

[25] L. Fan and X. Wang, "Internal model based iterative learning control for linear motor motion systems," in *Sixth International Conference on Intelligent Systems Design and Applications*, 2006.

[26] M. Butcher and A. Karimi, "Linear parameter-varying iterative learning control with application to a linear motor system," *IEEE/ASME Transactions on Mechatronics*, vol. 15, no. 3, pp. 412–420, 2010.

[27] Y. Koren and C. C. Lo, "Variable-gain cross-coupling controller for contouring," *CIRP Annals-Manufacturing Technology*, vol. 40, no. 1, pp. 371–374, 1991.

[28] Y. Koren, "Cross-coupled biaxial computer control for manufacturing systems," *Journal of Dynamic Systems, Measurement and Control*, vol. 102, no. 4, pp. 265–272, 1980.

[29] P. K. Kulkarni and K. Srinivasan, "Identification of discrete time dynamic time models for machine tool drives," in *Proc. of The Symposium on Sensors and Controls for Automated Manufacturing*, 1984.

[30] P. K. Kulkarni and K. Srinivasan, "Cross coupled compensators for contouring control of multi-axis machine tools," in *Proc. of the Thirteenth North American Manufacturing Research Conference*, 1985.

[31] P. K. Kulkarni, *Identification of Contouring Control of Multi-Axial Tool Feed Drives*. PhD thesis, Ohio State University, 1987.

[32] P. K. Kulkarni and K. Srinivasan, "Optimal contouring control of multi-axial feed drive servomechanisms," *ASME Journal of Engineering for Industry*, vol. 111, pp. 140–148, 1990.

[33] P. K. Kulkarni and K. Srinivasan, "Cross-coupled control of biaxial feed drive servomechanisms," *Journal of Dynamis Systems, Measurement and Control*, vol. 112, pp. 225–232, 1990.

[34] J. Yang, D. Zhang, and Z. Li, "Position loop-based cross-coupled control for high-speed machining," in *Proc. of the Seventeenth World Congress on Intelligent Control and Automation*, 2008.

[35] M. Naumovic and M. Stojic, "Design of the observer based cross-coupled positioning servodrives," in *Proc. of the IEEE International Symposium on Industrial Electronics, ISIE '97*, vol. 2, 1997.

[36] H. Y. Chuang and C. H. Liu, "A model referenced adaptive control strategy for improving contour accuracy of multi-axis machine tools," in *Conference Record of the 1990 IEEE Industry Applications Society Annual Meeting* (2, ed.), pp. 1539–1544, 1990.

[37] K. L. Barton and A. G. Alleyne, "Cross-coupled ilc for improved precision motion control: design and implementation," in *Proc. of The American Control Conference*, pp. 5496–5502, 2007.

[38] H. S. Li, X. Zhou, and Y. Chen, "Iterative learning control for cross-coupled contour motion systems," in *Mechatronics and Automation, 2005 IEEE International Conference*, vol. 3, pp. 1468–1472, 2005.

[39] A. E. Khalick and N. Uchiyama, "Contouring controller design based on iterative contour error estimation for three-dimensional machining," *Robotics and Computer-Integrated Manufacturing*, vol. 27, pp. 802–807, 2011.

[40] N. Gecer-Ulu, E. Ulu, and M. Cakmakci, "Learning based cross-coupled control for multi-axis high precision positioning systems," in *Proc. ASME Dynamic Systems and Control Conf. (DSCC 2012)*, (Ft. Lauderdale, FL), Oct 2012. To appear.

[41] S. S. Yeh and P. L. Hsu, "Theory and applications of the robust cross-coupled control design," in *Proc. of the American Control Conference*, pp. 791–795, 1997.

[42] H. Z. Li, Z. M. Gong, W. Lin, and T. Lippa, "Motion profile planning for reduced jerk and vibration residuals," tech. rep., SIMTech, 2007.

[43] B. G. Dijkstra, N. J. Rambaratsingh, C. W. Scherer, O. H. Bosgra, M. S. Steinbuch, and S. Kerssemakers, "Input design for optimal discrete time point to point motion of an industrial xy-positioning table," in *IEEE Conference on Desicion and Control.*

[44] C. W. Ha, K. H. Rew, and K. S. Kim, "A complete solution to asymmetric s-curve motion profile: theory and experiments," in *International Conference on Control, Automation and Systems*, 2008.

[45] D. A. Bristow and A. G. Alleyne, "A high precision motion control system with application to microscale robotic deposition," *IEEE Transactions on Control Systems Technology*, vol. 14, no. 6, pp. 1008–1020, 2006.

[46] S. M. Wang, Z. S. Chiang, D. F. Chen, and Y. Y. Tsai, "A new cutting force model for micromilling and determination of optimal cutting parameters," *Advanced Materials Research*, pp. 680–687, 2009.

Appendix A

Simulink Diagrams
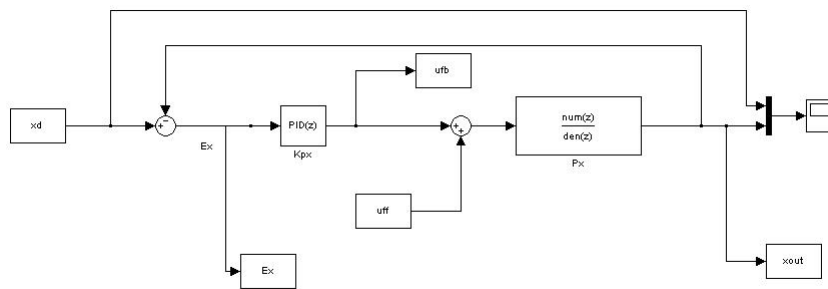
Figure A.1: Simulink Block Diagram for ILC
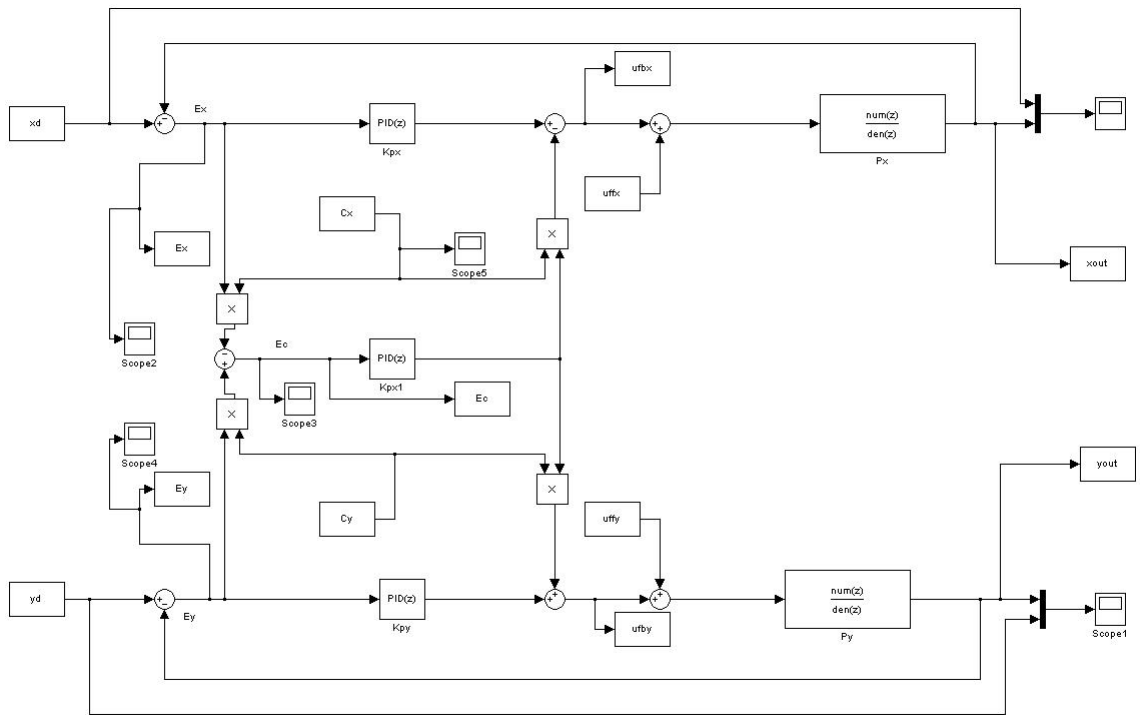
Figure A.2: Simulink Block Diagram for Learning Based Cross Coupled Control in Two-axis
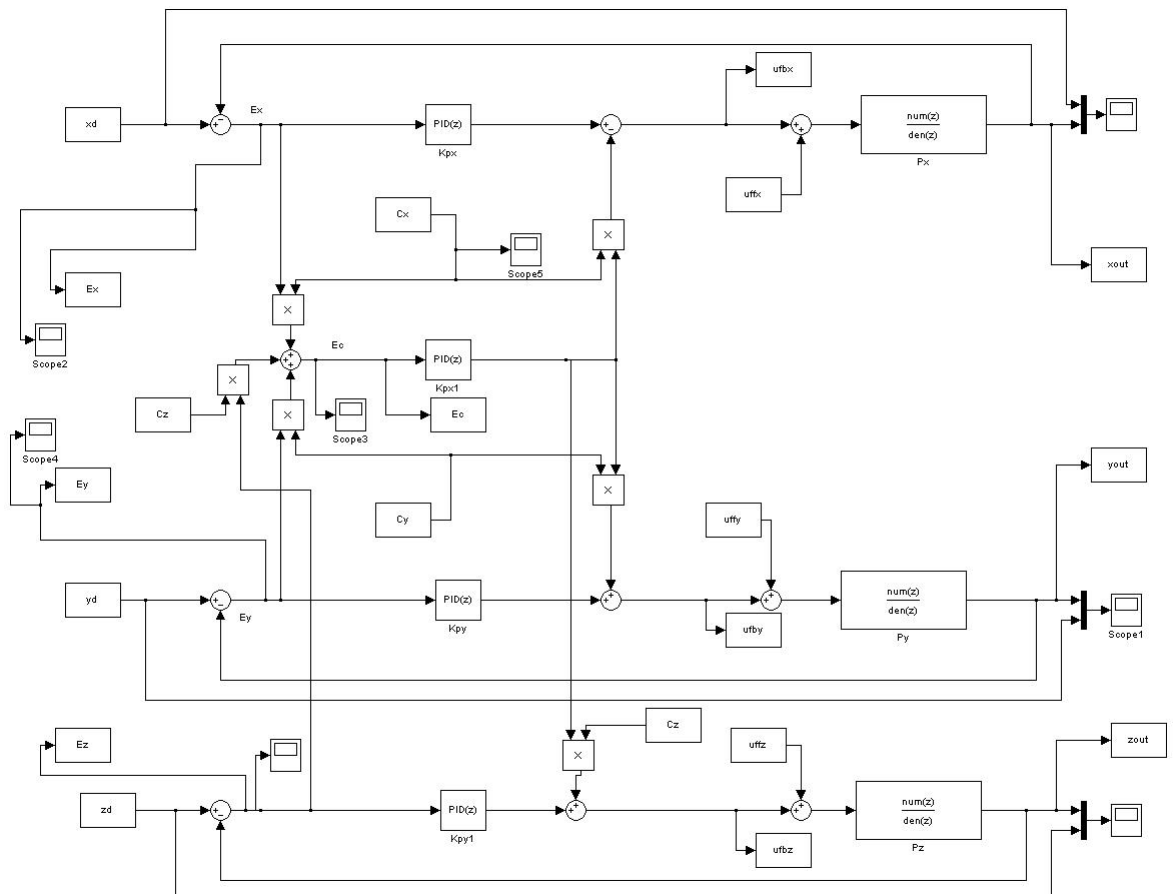
Figure A.3: Simulink Block Diagram for Learning Based Cross Coupled Control in Three-axis

Appendix B

Labview Implementations
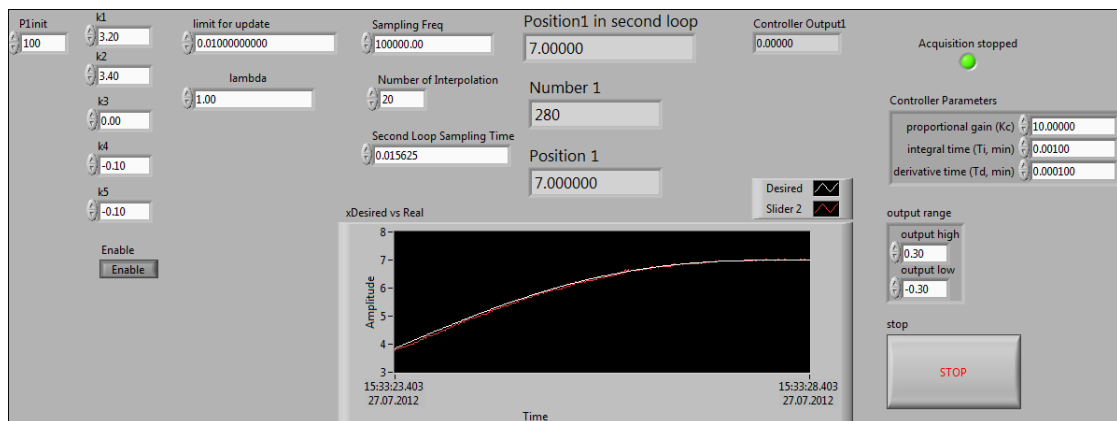
Figure B.1: Front Panel for Single-axis ILC Control
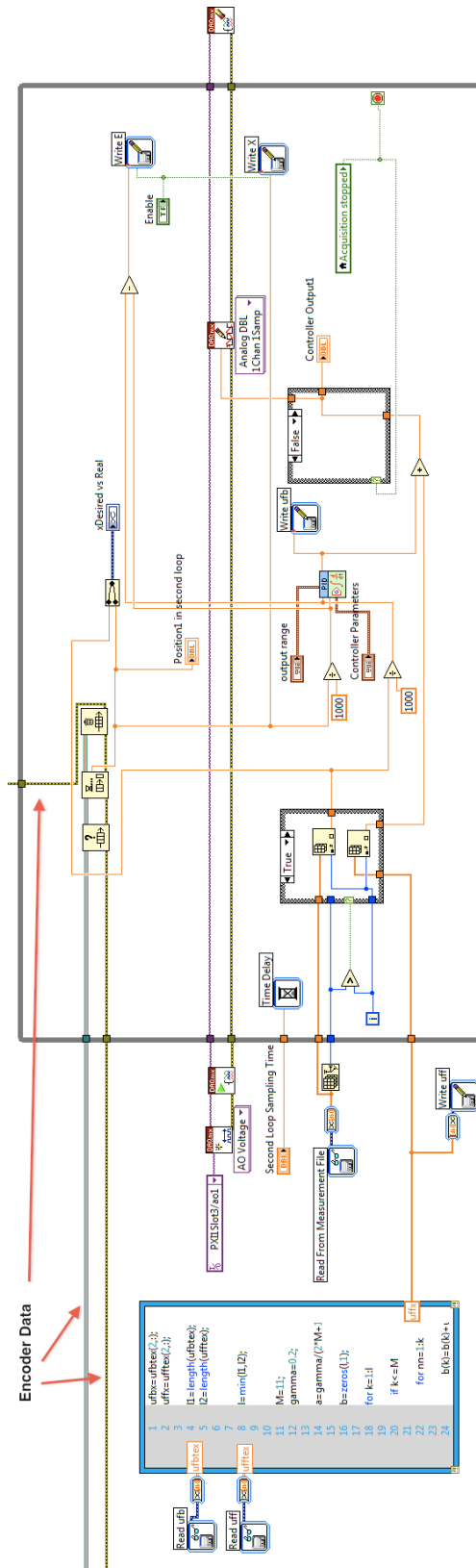
Figure B.2: Labview VI for Single-axis ILC Control

75
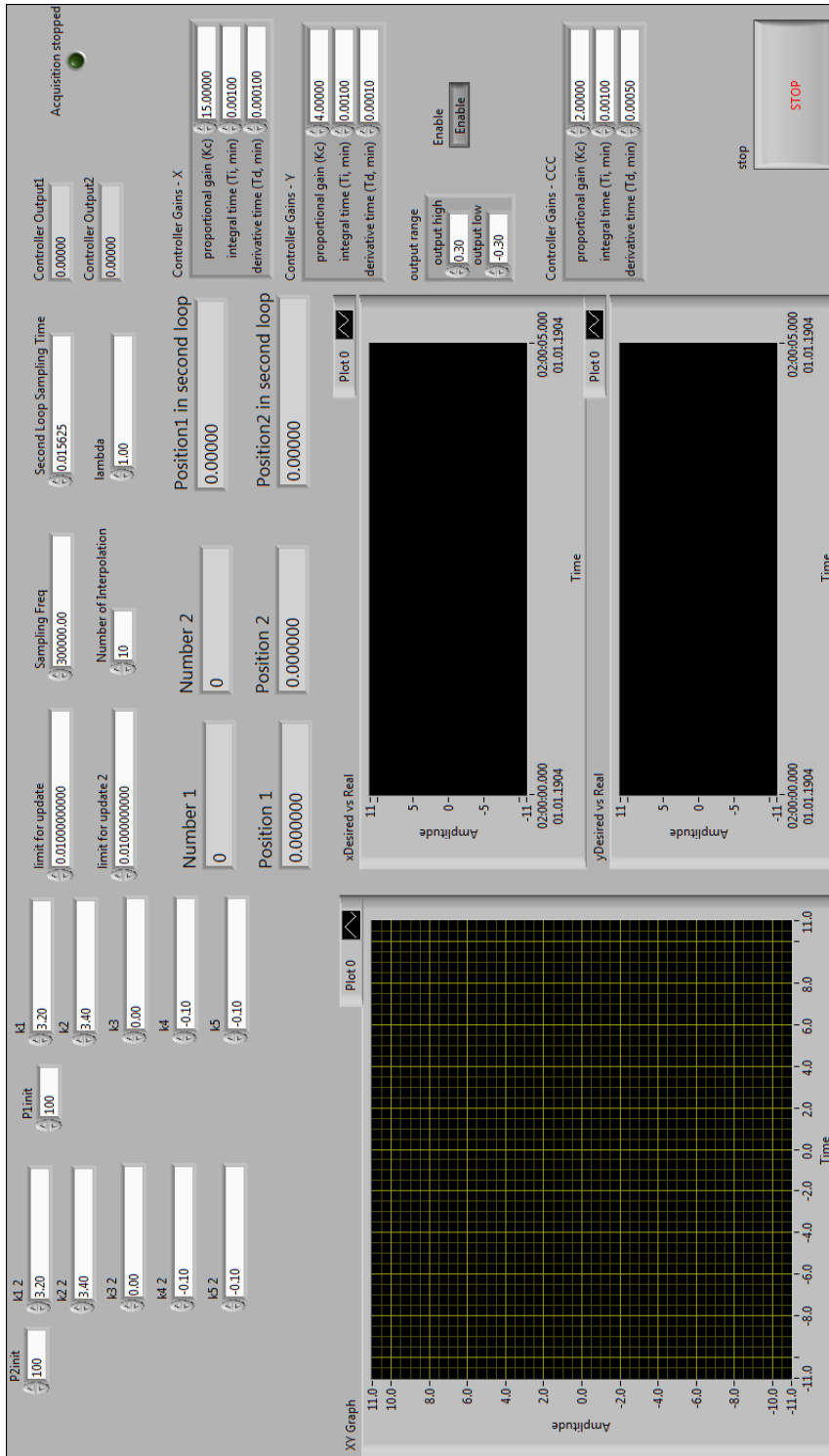
Figure B.3: Front Panel for Two-axis Learning Based Cross-coupled Control
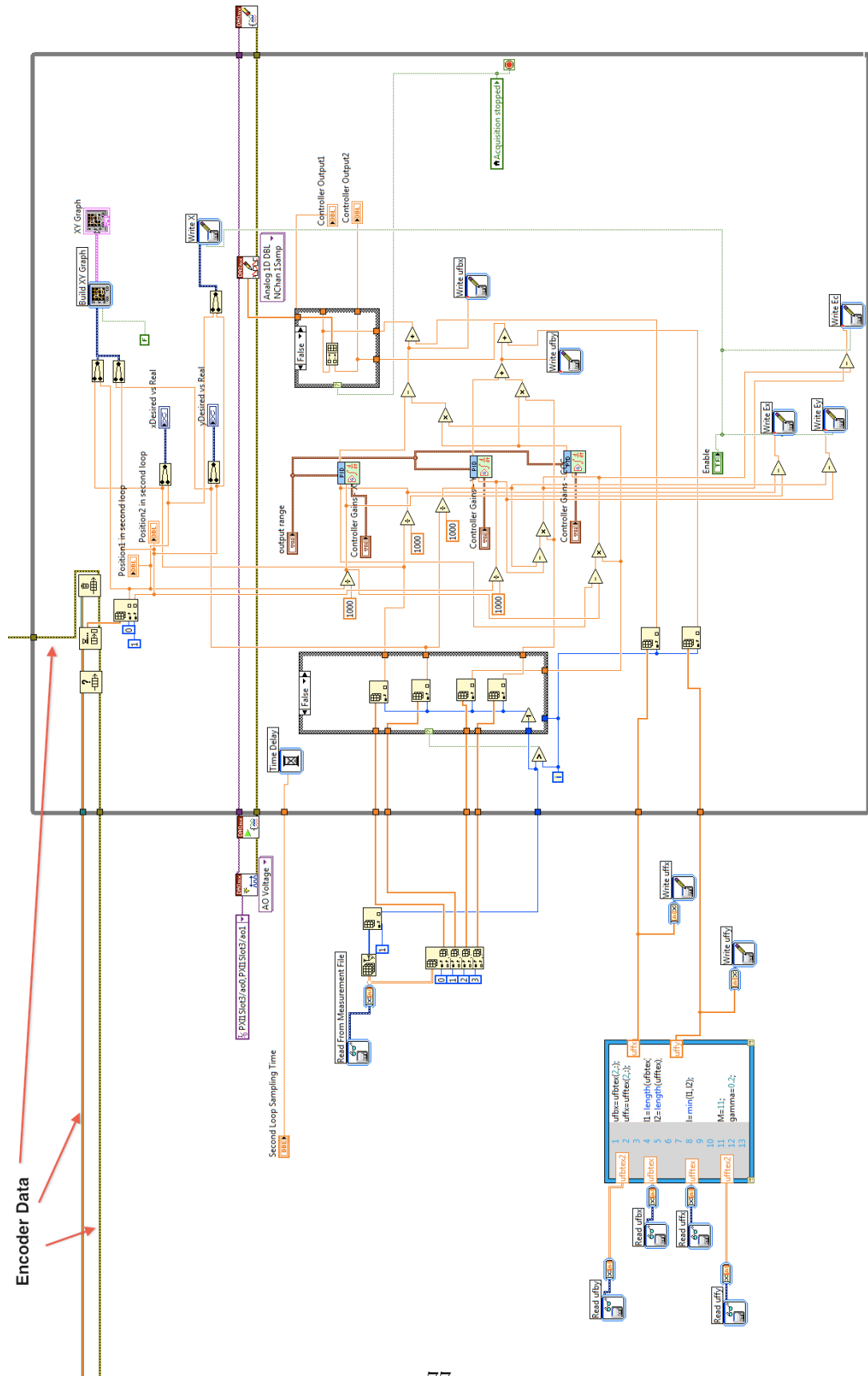
Figure B.4: Labview VI for Two-axis Learning Based Cross-coupled Control
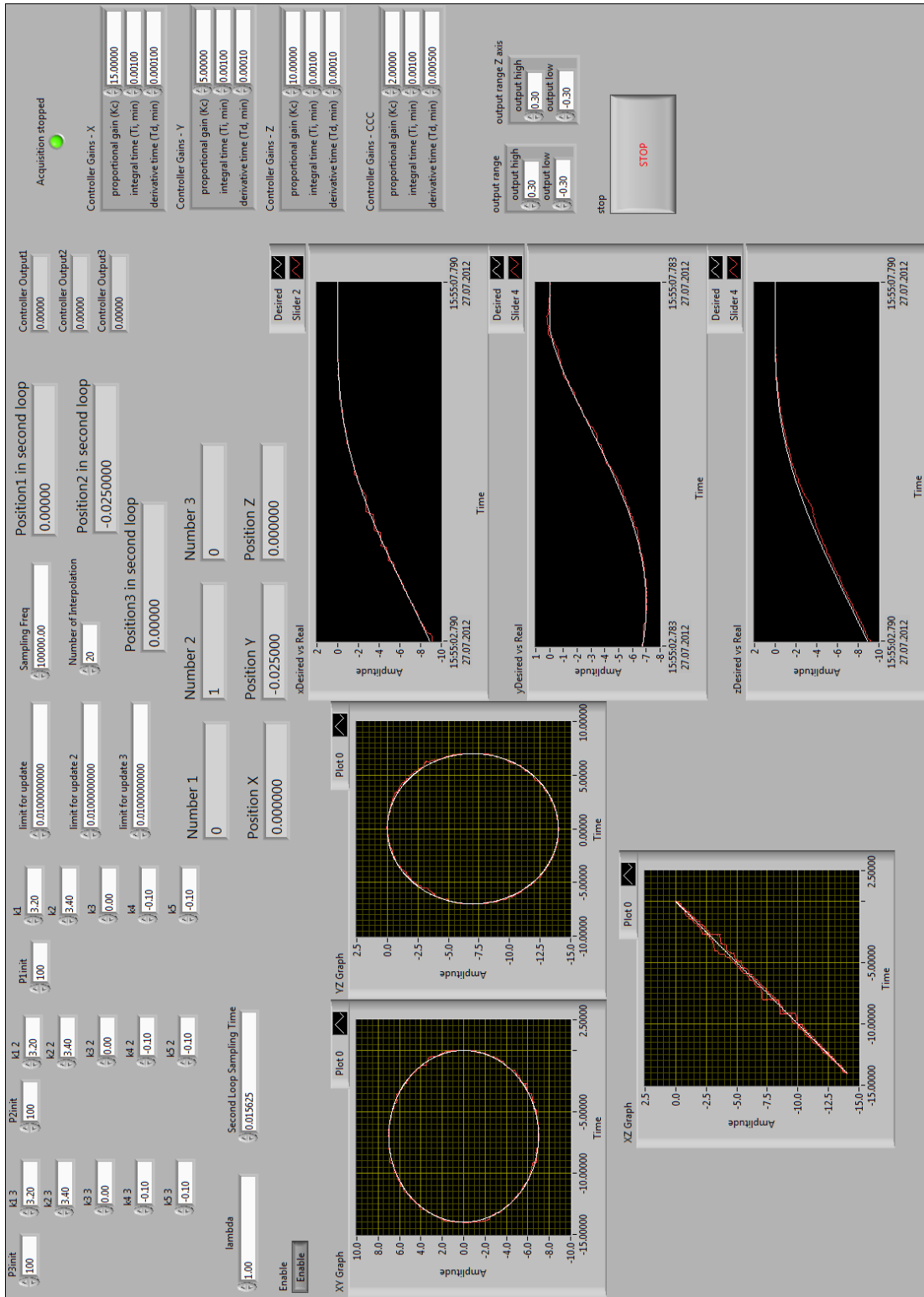
Figure B.5: Front Panel for Three-axis Learning Based Cross-coupled Control
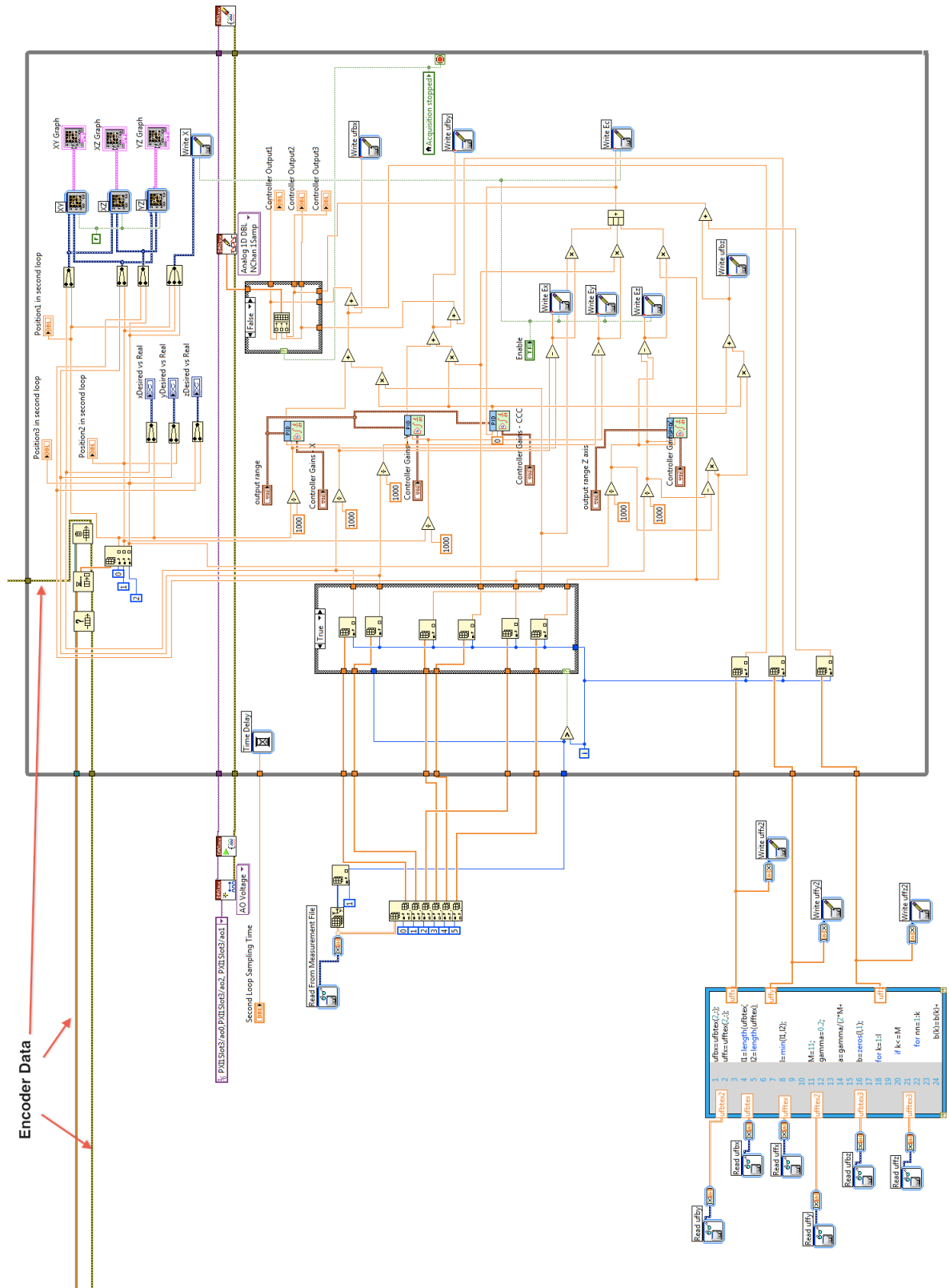
Figure B.6: Labview VI for Three-axis Learning Based Cross-coupled Control

Appendix C

Trajectories
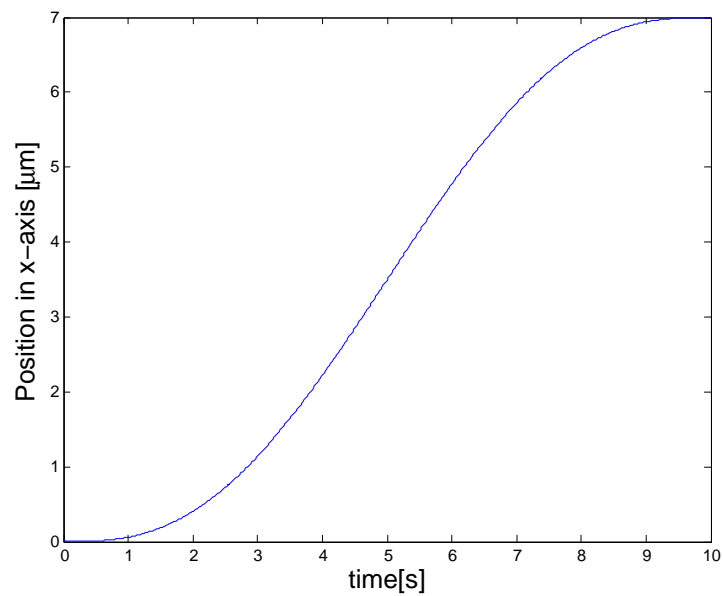
Figure C.1: Trajectory for single-axis simulations and experiments
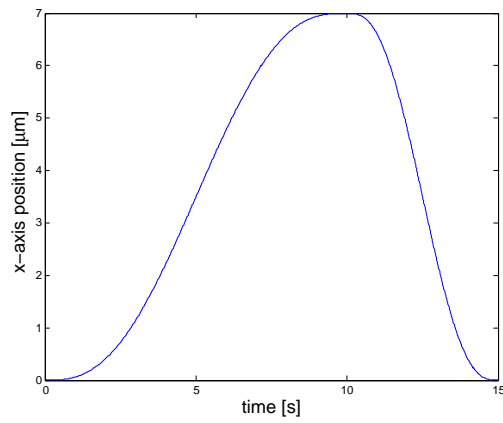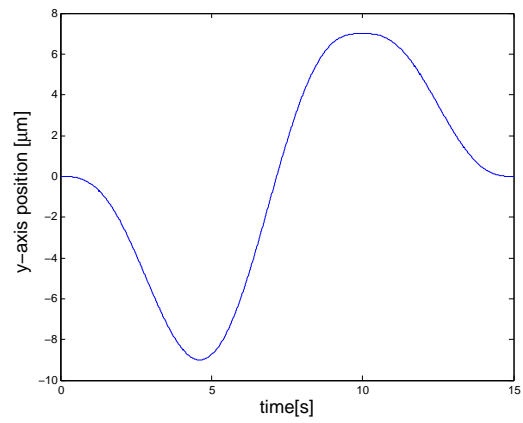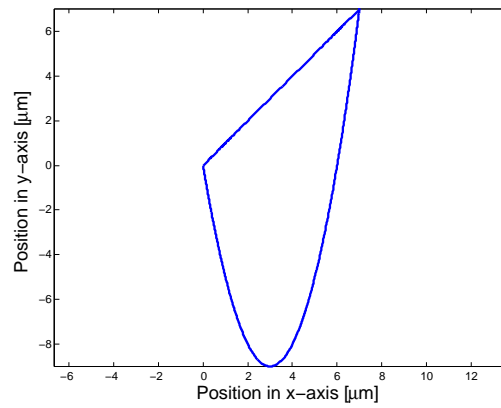
Figure C.2: (a) x-axis trajectory, (b) y-axis trajectory and (c) contour for the two-axis simulation and experiments
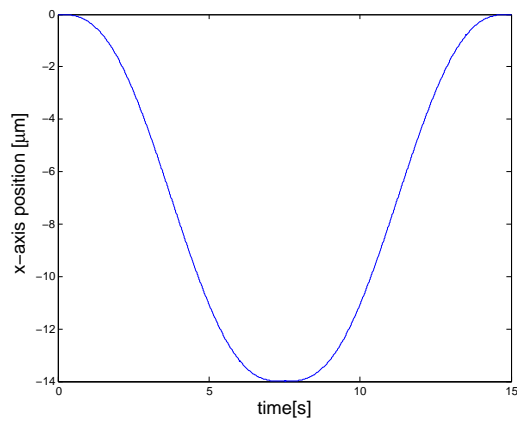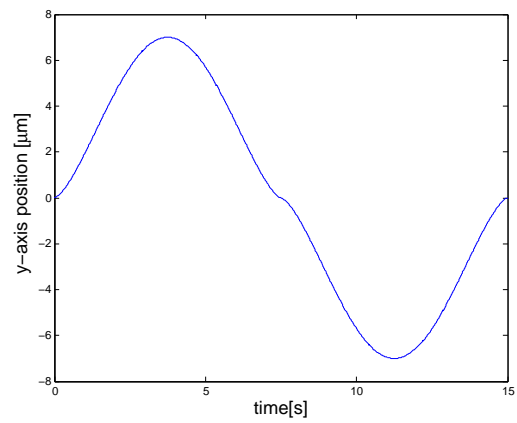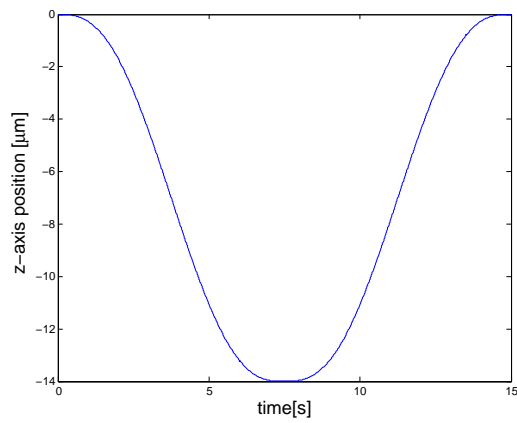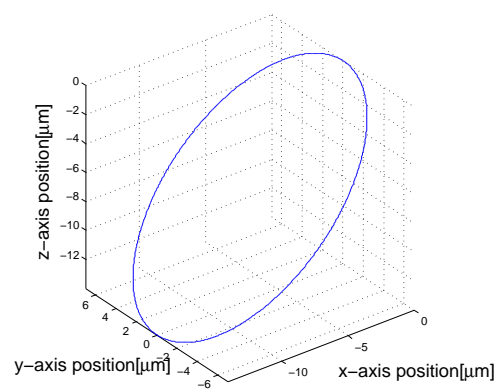
Figure C.3: (a) x-axis trajectory, (b) y-axis trajectory, (c) z-axis trajectory and (d) contour for the three-axis simulation and experiments